The Neutrino Magnetic Moment Portal:
Cosmology, Astrophysics, and Direct Detection

Vedran Brdar,[1, a] Admir Greljo,[2, b] Joachim Kopp,[2, 3, c] and Toby Opferkuch[2, d]

[1]*Max Planck-Institut für Kernphysik, Saupfercheckweg 1, 69117 Heidelberg, Germany*
[2]*Theoretical Physics Department, CERN, 1 Esplanade des Particules, 1211 Geneva 23, Switzerland*
[3]*PRISMA Cluster of Excellence & Mainz Institute for Theoretical Physics,*
Johannes Gutenberg University, Staudingerweg 7, 55099 Mainz, Germany

We revisit the physics of neutrino magnetic moments, focusing in particular on the case where the right-handed, or sterile, neutrinos are heavier (up to several MeV) than the left-handed Standard Model neutrinos. The discussion is centered around the idea of detecting an upscattering event mediated by a transition magnetic moment in a neutrino or dark matter experiment. Considering neutrinos from all known sources, as well as including all available data from XENON1T and Borexino, we derive the strongest up-to-date exclusion limits on the active-to-sterile neutrino transition magnetic moment. We then study complementary constraints from astrophysics and cosmology, performing, in particular, a thorough analysis of BBN. We find that these data sets scrutinize most of the relevant parameter space. Explaining the XENON1T excess with transition magnetic moments is marginally possible if very conservative assumptions are adopted regarding the supernova 1987 A and CMB constraints. Finally, we discuss model-building challenges that arise in scenarios that feature large magnetic moments while keeping neutrino masses well below 1 eV. We present a successful ultraviolet-complete model of this type based on TeV-scale leptoquarks, establishing links with muon magnetic moment, B physics anomalies, and collider searches at the LHC.

I. INTRODUCTION

When dark matter detection using nuclear recoils was first proposed by Goodman and Witten in 1985 [1], the idea was presented as a parasitical measurement in a neutrino detector proposed a few months earlier [2]. Since then, direct dark matter searches have turned into a vast field of research in its own right, with numerous advanced experiments and with a community numbering in the thousands. With the current generation of detectors, the circle closes as dark matter experiments are becoming sensitive probes of low-energy neutrino physics. In particular, experimental sensitivities are approaching the so-called "neutrino floor", an unavoidable background due to scattering of solar and atmospheric neutrinos [3–5]. The resulting nuclear and electronic recoils are in general indistinguishable from a dark matter signal, and are therefore often characterized as a severe limitation to dark matter searches. On the other hand, precision measurements of the neutrino floor also offer tremendous discovery opportunities for phenomena beyond the Standard Model (SM) in neutrino physics [4].

In this work, we focus in particular on neutrino magnetic moments, which are predicted to be tiny ($<$ $10^{-19} \mu_\mathrm{B}$) in the SM [6–13], but can be substantially larger in theories beyond the SM [10, 12, 14–18]. The possibility that neutrino magnetic moments enhance the neutrino floor in direct dark matter detection experiments has been discussed for quite some time [4], but

only now experiments are reaching the sensitivity to set meaningful constraints [19].

In view of these new experimental opportunities, our goals in this paper are the following: in section II, we discuss the event spectra for solar neutrinos recoiling against electrons and nuclei in the presence of large neutrino magnetic moments. Unlike much of the previous literature, we allow the mass of the right-handed neutrinos to be much larger than the mass of their left-handed partners, so that magnetic moment-induced scattering processes $\nu_L + e^- \to N_R + e^-$ and $\nu_L + X_Z^A \to N_R + X_Z^A$ can be inelastic. Here, N_R denotes the right-handed (sterile) neutrinos, and X_Z^A is an atomic nucleus. This well-motivated possibility opens up significant new parameter space. We use our event spectra to derive limits from XENON1T and Borexino data [19, 20], and to predict the sensitivity of future observatories like DARWIN. We also show that the excess electron recoil events reported in ref. [19] can be explained by neutrino transition magnetic moments. This possibility has also been considered in refs. [17, 21], but compared to these papers, we will employ a much more detailed fit, including a more sophisticated treatment of backgrounds and covering a much larger recoil energy range. We find qualitative differences compared to the results of ref. [21], and we will discuss their origin. It is worth mentioning that after the announcement of the XENON1T excess in ref. [19], an avalanche of papers has appeared offering various explanations of the anomaly. Without being exhaustive, let us mention a couple of promising scenarios, namely dark photons [22–24]), inelastic dark matter down-scattering [25–27] and light dark matter decay [28]. A proposed explanation in terms of solar axions is more difficult to realize, though see [23, 29, 30].

We will also go well beyond refs. [17, 21] in section III,

[a] vbrdar@mpi-hd.mpg.de
[b] admir.greljo@cern.ch
[c] jkopp@cern.ch
[d] toby.opferkuch@cern.ch

where we discuss a comprehensive set of constraints on neutrino magnetic moments. In particular, we show how astrophysical observations (stellar cooling, supernova 1987A), cosmological measurements (BBN, CMB), and terrestrial experiments (neutrino scattering) disfavor vast regions of parameter space, while nevertheless leaving large swathes open. We present in particular detailed simulations of Big Bang Nucleosynthesis (BBN) in the presence of neutrino magnetic moments. We also outline model-building strategies for avoiding these constraints, showing that some options are quite simple, while others are fairly exotic. In the final part of the paper, section IV, we depart from the effective field theory (EFT) description of neutrino magnetic moments and discuss ultraviolet (UV) completions. Typically, large neutrino magnetic moments require fine-tuning to avoid large corrections to the neutrino masses. We show explicit models featuring TeV-scale leptoquarks, partially motivated by various anomalies in B physics, which elegantly avoid this problem.

We will summarize our results and conclude in section V.

II. NEUTRINO MAGNETIC MOMENTS AND DIRECT DARK MATTER SEARCHES

A. Modified Solar Neutrino Spectrum

Neutrino magnetic moments are described at low energies by the effective operator,

$$\mathcal{L}_\mu = \frac{\mu_\nu^\alpha}{2} F_{\mu\nu} \bar{\nu}_L^\alpha \sigma^{\mu\nu} N_R + \text{h.c.}, \tag{1}$$

where $F^{\mu\nu}$ is the electromagnetic field strength tensor, N_R is a right-handed neutrino gauge singlet, and ν_L^α is the SM neutrino field of flavor α. In this paper, we will assume transition magnetic moments between ν_μ and N_R unless otherwise stated. This is motivated by the UV completions we consider in section IV. To simplify our notation, we will omit the superscript α in the following. The factor $\frac{1}{2}$ in eq. (1) is a convention usually adopted in the literature. We imagine that the operator in eq. (1) originates from short-distance new physics above the electroweak scale which generates the following gauge-invariant operators

$$\mathcal{L} \supset \frac{c_B}{\Lambda^2} g' B_{\mu\nu} \bar{L}_L \tilde{H} \sigma^{\mu\nu} N_R + \frac{c_W}{\Lambda^2} g W_{\mu\nu}^a \bar{L}_L \sigma^a \tilde{H} \sigma^{\mu\nu} N_R. \tag{2}$$

Here g (g') is the $SU(2)_L$ (hypercharge) gauge coupling, Λ is the cutoff scale, L_L denotes a SM lepton doublet, $W_{\mu\nu}^a$ ($B_{\mu\nu}$) is the $SU(2)_L$ (hypercharge) field strength tensor, σ^a are Pauli matrices, and $\tilde{H} \equiv i\sigma^2 H^*$ is the conjugate Higgs field. After electroweak symmetry breaking, the neutrino magnetic moment becomes

$$\mu_\nu = \frac{\sqrt{2}e\,v_H}{\Lambda^2} (c_B + c_W), \tag{3}$$

with the Higgs vacuum expectation value v_H and the electromagnetic gauge coupling e. The operator in eq. (1) mediates neutrino–electron scattering, $\nu_L + e^- \to N_R + e^-$, as well as neutrino–nucleus scattering, $\nu_L + X_Z^A \to N_R + X_Z^A$. Since the masses of ν_L and N_R can in general be different, the scattering may be inelastic. The differential scattering rates for the two processes are [4, 31–35]

$$\frac{d\sigma_\mu(\nu_L e \to N_R e)}{dE_r} = \alpha\mu_\nu^2 \left[\frac{1}{E_r} - \frac{1}{E_\nu} + M_N^2 \frac{E_r - 2E_\nu - m_e}{4E_\nu^2 E_r m_e} + M_N^4 \frac{E_r - m_e}{8E_\nu^2 E_r^2 m_e^2} \right] \tag{4}$$

and

$$\frac{d\sigma_\mu(\nu_L X_Z^A \to N_R X_Z^A)}{dE_r} = \alpha\mu_\nu^2 Z^2 F_1^2(E_r) \left[\frac{1}{E_r} - \frac{1}{E_\nu} + M_N^2 \frac{E_r - 2E_\nu - m_X}{4E_\nu^2 E_r m_X} + M_N^4 \frac{E_r - m_X}{8E_\nu^2 E_r^2 m_X^2} \right]$$
$$+ \alpha\mu_\nu^2 \mu_X^2 F_2^2(E_r) \left[\frac{2m_X}{E_\nu^2} \left((2E_\nu - E_r)^2 - 2E_r m_X \right) + M_N^2 \frac{E_r - 4E_\nu}{E_\nu^2} + M_N^4 \frac{1}{E_\nu^2 E_r} \right]. \tag{5}$$

Here, M_N is the right-handed neutrino mass, α is the electromagnetic fine structure constant, E_ν is the neutrino energy, E_r is the electron or nuclear recoil energy, and Z is the nuclear charge in units of e. Also, m_X and μ_X are the nuclear mass and magnetic moment, respectively, while A is the number of nucleons. The term in the first line of eq. (5) contains an enhancement factor Z^2 because in low-energy scattering the neutrino interacts with the whole nucleus coherently. At higher energies, the substructure of the nucleus is partly resolved and coherence is broken. This is described by the nuclear charge and magnetic form factors $F_1(E_r)$, $F_2(E_r)$. The charge form factor can be parameterized as $F_1(E_r) = 3e^{-\kappa^2 s^2/2}[\sin(\kappa r) - \kappa r \cos(\kappa r)]/(\kappa r)^3$, with $s = 1\,\text{fm}$, $r = \sqrt{R^2 - 5s^2}$, $R = 1.2A^{1/3}\,\text{fm}$, $\kappa = \sqrt{2m_X E_r}$ (and $q^2 \simeq -\kappa^2$) [36]. For the magnetic form factor, no such general parameterization exists. In the following, we will *neglect* nuclear magnetic moments (and thus the

whole second line of eq. (5)) because scattering on the nuclear magnetic moment is strongly suppressed compared to scattering on the nuclear charge due to the absence of Z^2 enhancement.

Equations (4) and (5) should be compared to the corresponding expressions for neutrino–electron scattering and neutrino–nucleus scattering in the Standard Model [3, 4, 37, 38]:

$$\frac{d\sigma_{\rm SM}(\nu_e e \to \nu_e e)}{dE_r} = \frac{G_F^2 m_e}{2\pi E_\nu^2}\left[4s_w^4(2E_\nu^2 + E_r^2 - E_r(2E_\nu + m_e)) - 2s_w^2(E_r m_e - 2E_\nu^2) + E_\nu^2\right], \quad (6)$$

$$\frac{d\sigma_{\rm SM}(\nu_{\mu,\tau} e \to \nu_{\mu,\tau} e)}{dE_r} = \frac{G_F^2 m_e}{2\pi E_\nu^2}\left[4s_w^4(2E_\nu^2 + E_r^2 - E_r(2E_\nu + m_e)) + 2s_w^2(E_r m_e - 2E_\nu^2) + E_\nu^2\right], \quad (7)$$

$$\frac{d\sigma_{\rm SM}(\nu_{e,\mu,\tau} X_Z^A \to \nu_{e,\mu,\tau} X_Z^A)}{dE_r} = \frac{G_F^2 m_X Q_w^2 F^2(E_r)}{8\pi E_\nu^2}\left[2E_\nu^2 - 2E_\nu E_r - E_r m_X\right]. \quad (8)$$

In the last expression, $Q_w = 2T_3 - 4Z\sin^2\theta_w$ is the weak charge of the nucleus, which depends on its weak isospin $T_3 = (2Z - A)/2$. As eq. (8) accounts only for the vector couplings of the Z boson, but not its axial-vector interactions, this expression is strictly valid only for spin-0 nuclei. We will, however, use it also for nuclei with non-zero spin because vector interactions always dominate for heavy nuclei thanks to the enhancement by Q_w^2. Axial-vector couplings do not profit from such an enhancement because the contributions from different nucleons tend to cancel, rather than adding up coherently like for the vector couplings.

Note that in the literature, the term $2E_\nu E_r$ in eq. (8) is often dropped because it is much smaller than the other two terms at the recoil energies of experimental interest. In some references, an extra term E_r^2 is included inside the square brackets. This term arises when the nucleus is treated as a spin-1/2 fermion, but it should be omitted for spin-0 nuclei. In any case, this extra term is usually negligibly small compared to the others.

The event rate is obtained from the differential cross section $d\sigma/dE_r$ according to [4]

$$\frac{dR}{dE_r} = N_T \epsilon(E_r) \int_{E_\nu^{\rm min}} dE_\nu \frac{d\Phi}{dE_\nu}\frac{d\sigma}{dE_r}, \quad (9)$$

where N_T is the number of target electrons, $\epsilon(E_r)$ is the detection efficiency, and $d\Phi/dE_\nu$ is the neutrino flux. We adopt the solar neutrino flux from the BS05(OP) Standard Solar Model (SSM) introduced in ref. [39]. As we will mostly assume that only one of the active neutrino flavors participates in the magnetic moment interactions, we need to include also neutrino oscillations. We do so following the standard approach (see for instance ref. [40]), assuming fully adiabatic flavor transitions. The lower integration boundary in eq. (9) is the minimum neutrino energy required to attain a recoil energy E_r,

$$E_\nu^{\rm min}(E_r) = \frac{1}{2}\left[E_r + \sqrt{E_r^2 + 2m_e E_r}\right]\left(1 + \frac{M_N^2}{2E_r m_e}\right). \quad (10)$$

In fig. 1 we compare the electron and nuclear recoil rates in the SM to those predicted in the presence of non-zero neutrino magnetic moments, for two combinations of (M_N, μ_ν). For the case of massless or very light N_R (blue curve), the scaling with $1/E_r$ at low recoil energies predicted by eqs. (4) and (5) is evident. The chosen value of $\mu_\nu = 5.7 \times 10^{-11}\,\mu_{\rm B}$ corresponds to the best fit point to the XENON1T low-energy excess (see section II B below). It is important, however, to emphasize, that the stellar cooling limits discussed below in section III A disfavor such large μ_ν by more than an order of magnitude [41] for $M_N \lesssim 20\,{\rm keV}$.

If M_N is larger, comparable to the center-of-mass energy $\sqrt{s} = \sqrt{m_e^2 + 2E_\nu m_e}$, the magnetic moment-induced recoil spectrum changes shape: it vanishes below

$$E_r^{\rm min} = \frac{M_N^2}{2(m_e + M_N)} \quad (11)$$

because no kinematic solutions exist for any E_ν. At higher E_r, the spectrum gradually increases before reaching a maximum, which for a monochromatic neutrino flux is located at a recoil energy of

$$E_r^{\rm peak}(E_\nu) = \frac{2m_e M_N^4}{8E_\nu^2 m_e^2 - 2m_e M_N^2(2E_\nu + m_e) + M_N^4}. \quad (12)$$

The maximum possible recoil energy for a given neutrino energy E_ν is reached at

$$E_r^{\rm max}(E_\nu) = \frac{1}{2E_\nu + m_e}\left[E_\nu^2 - \tfrac{1}{2}M_N^2 \right.$$
$$\left. + \frac{E_\nu}{2m_e}\left(\sqrt{M_N^4 - 4M_N^2 m_e(E_\nu + m_e) + 4E_\nu^2 m_e^2} - M_N^2\right)\right]. \quad (13)$$

As different components of the solar neutrino spectrum switch on at different values of E_r (see eq. (10)), the event spectrum strongly depends on M_N whenever $M_N^2/(2E_r m_e) \gtrsim 1$. In fig. 1, we illustrate this by showing the spectrum for one representative parameter point
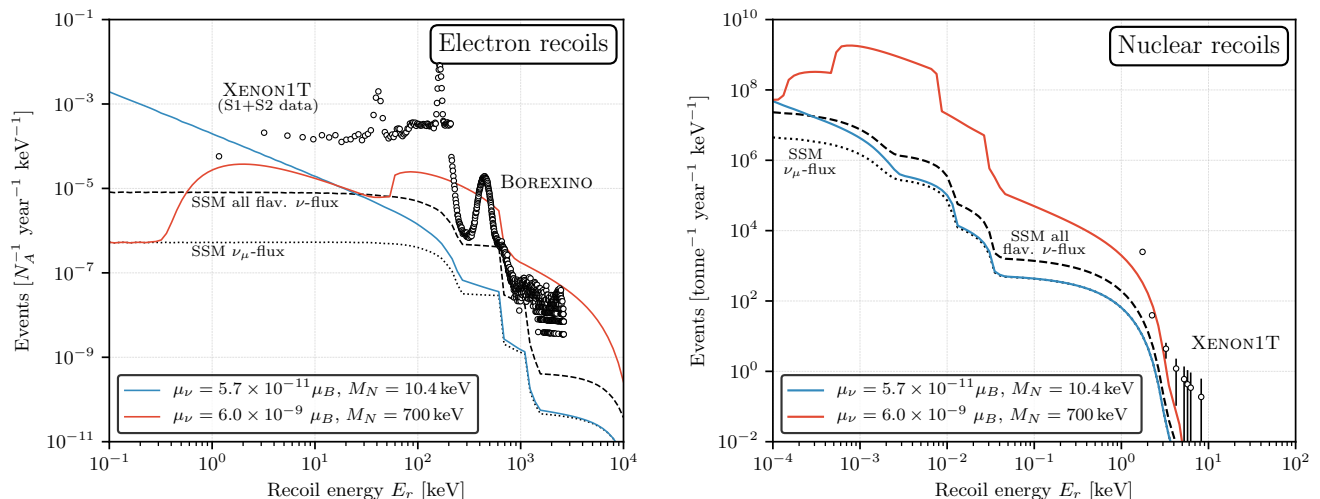
FIG. 1. The rate of neutrino-induced electron recoils (left) and nuclear recoils (right) in a dark matter detector for the Standard Model (black curves) and for scenarios with enhanced neutrino magnetic moments (colored curves). We also include data points from XENON1T [19] and Borexino [20] for comparison. For very light right-handed neutrinos, we observe the $1/E_r$ scaling predicted by eqs. (4) and (5) in that limit. For larger M_N, the predicted recoil spectrum has a broad bump, and the interplay of eqs. (4) and (5) with the shape of the solar neutrino spectrum leads to interesting spectral features.

with large M_N (red curve). For the chosen case, the XENON1T excess is accommodated by the ^{7}Be neutrino flux, and the higher-energy CNO, pep, ^{8}B, and hep fluxes lead to a substantial number of recoil events also at higher energies. While these higher-energy events are also visible in XENON1T, they are probed with much greater sensitivity by Borexino, as can be seen by comparing to the XENON1T and Borexino data points which we have included in fig. 1 for comparison. This example illustrates the more general statement that XENON1T will be most sensitive at low M_N, while Borexino is in a better position to constrain models with $M_N \gtrsim \mathcal{O}(100\,\text{keV})$.

B. XENON1T

To compare the predicted magnetic moment signals in XENON1T to the data more quantitatively, we have carried out maximum-likelihood fit to both electron recoil and nuclear recoil data. Electron recoils in XENON1T have recently attracted significant attention due to a $\sim 3\sigma$ excess over background [19], while nuclear recoils are the main channel for direct detection of Weakly Interacting Massive Particle (WIMP) dark matter, and the channel for which dark matter detectors are optimized [42].

We use binned electron recoil event rates in the complete energy range from zero to 210 keV. For the low energy range we use the data from fig. 4 of ref. [19], while for the range from 30 to 210 keV we take the data from fig. 3 of the same reference. The background predictions for the individual components are again lifted from fig. 3 of ref. [19], but in the fit we allow their normalization to

float within the uncertainties listed in Table I of ref. [19]. The neutrino signal is composed of the SM weak scattering processes described by eqs. (6) and (7), and of the new physics piece given by eq. (4).

The event rate follows eq. (9), with the detection efficiencies taken from Fig. 2 of ref. [19]. To obtain N_T for the case of XENON1T, we sum over all stable isotopes of xenon, weighted by their natural abundances. After computing the expected count rates according to eq. (9), we apply Gaussian smearing based on the detector resolution given in fig. 2 of the supplemental material to ref. [43].

For predicting the rate of nuclear recoils in XENON1T, we construct bins in E_r from the S1 (scintillation) and S2 (ionization) signals, see fig. 3 in ref. [42]. The data of interest lies in the nuclear recoil signal region in this figure. We employ Poissonian smearing in S1. The number of photoelectrons in the S2 channels is much larger than in the S1 channel, so the relative importance of Poisson fluctuations in that channel is much smaller, so we neglect it. The most relevant background process arises from neutrons [44], which we include in our likelihood analysis. Detection efficiencies are taken from fig. 1 of ref. [42].

The results of our fit to XENON1T data are shown in fig. 2. At low M_N, our fit to electron recoil data is consistent with the one carried out by the XENON collaboration in ref. [19], but note that we have here assumed that only ν_μ participate in the magnetic moment interaction, whereas the XENON1T collaboration has assumed flavor-universal couplings. XENON1T Constraints on transition magnetic moments involving ν_e and ν_τ are similar to the ones for ν_μ. We find that magnetic
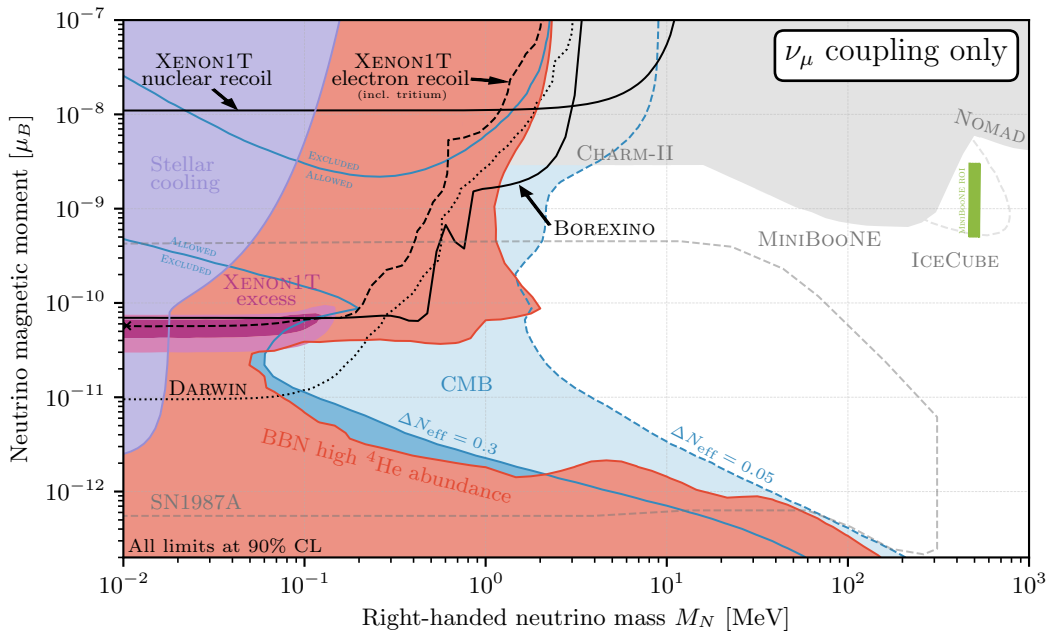
FIG. 2. Allowed 90% CL regions of the ν_μ–N transition magnetic moment as a function of the right-handed neutrino mass M_N. We compare the XENON1T exclusion contour including a possible tritium contamination (black dashed1) to the limits we obtain from Borexino data (black solid) and to the projected sensitivity of DARWIN [45]. We also show in pink the 1σ and 2σ regions preferred by the XENON1T excess in the absence of tritium contamination [19]. We see that the excess region is consistent with constraints from stellar cooling (purple region, see section III A) and BBN (red shaded region, see section III C 1), as well as a conservative CMB constraint on N_{eff} (blue shaded region, see section III C 2). The motivation for considering this more conservative constraint is the fact that larger N_{eff} is preferred by local measurements of the Hubble constant H_0. A less conservative CMB constraint (light blue) is in tension with the XENON1T-preferred region. The constraint from SN1987A (dashed gray contours) could be in tension with XENON1T as well, but we emphasize that this constraint may not be robust (see ref. [46], reviewed in section III B). We finally include terrestrial constraints (gray region at the top of the plot), taken from ref. [32, 35] as well as sensitivity projections for Icecube [35] (dashed) and the region preferred by MiniBooNE data (green) [32].

moments $\mu_\nu \gtrsim 7 \times 10^{-11}\,\mu_B$ are disfavored, and that the observed excess is well explained for μ_ν slightly below that value. Going beyond the analysis in ref. [19], we find that the sensitivity deteriorates at $M_N \gtrsim 200\,\text{keV}$ as the lowest energy solar neutrinos no longer have sufficient energy to create N_R.

Comparing our results to ref. [21], we find a slightly larger best fit value for μ_ν at low M_N, which can again be understood from our assumption that only ν_μ feel the magnetic moment interaction. At higher M_N, the authors of ref. [21] find secondary best fit regions, the most prominent of which lies at $M_N \simeq 600\,\text{keV}$ and $\mu_\nu \simeq 2 \times 10^{-9}\,\mu_B$. Interactions in this secondary region would be dominated by ^{8}B neutrinos. This region does not appear in our results due to enhancements of the spectrum at recoil energies $> 30\,\text{keV}$, see for instance the red curve in fig. 1. The plateau at $\sim 100\,\text{keV}$ that disfavors the $M_N \simeq 600\,\text{keV}$ solution in our fit is driven by the pep neutrino flux.

We have also entertained the likely possibility that the XENON1T excess is not a sign of new physics, but of some yet unknown SM background. Following the

XENON1T collaboration [19], we use tritium decays as a proxy for such a background, Including this background in our fit, we find the 90% CL limit shown in fig. 2 as a dashed black line. In the future, we expect this limit to improve by about a factor 4 with the DARWIN experiment [45]. We have computed the sensitivity of DARWIN assuming the same background model as in XENON1T (including tritium) and an exposure of $200\,\text{t}\cdot\text{years}$. The result is shown as a black dotted curve in fig. 2.

N_R masses up to several tens of MeV are in principle accessible using nuclear recoils in direct detection experiments, but the reach in μ_ν is much poorer in this case. The resulting limit is shown as a black curve in fig. 2 and has been cross-checked against a limit derived using Bayesian statistics in ref. [33].

Comparing to astrophysical and cosmological constraints, we find that the parameter region most interesting to direct detection experiments is only partially probed by stellar cooling constraints. At $M_N \gtrsim 20\,\text{keV}$, these constraints become unimportant as production of such heavy N_R is suppressed even in the hot cores of red giant stars. XENON1T's preferred region is in possible

tension with the anomalous cooling constraint from supernova 1987A and with the CMB measurement of N_{eff} (the effective number of relativistic degrees of freedom at recombination). We will discuss these constraints in more detail in section III, but we mention already here why these limits do not necessarily spoil the explanation of the XENON1T excess in terms of neutrino transition magnetic moments. For SN1987A, the argument is based on ref. [46], which argues that the observed neutrino signal from SN1987A might not have been from the cooling core, but rather from matter being accreted onto that core. Such a neutrino flux would not be significantly altered in the presence of N_R. For N_{eff}, early Universe observables (Planck, Baryon Acoustic Oscillations) considered in isolation prefer a value very close to 3 (dashed blue contour in fig. 2) [47]. Considering, however, late-time measurements of the Hubble constant H_0, somewhat larger values are preferred as they help relax the tension between late-time and early-time measurements of H_0 [48, 49]. Another very strong constraint is imposed by BBN (red shaded region in fig. 2, see section III C 1 for details). This constraint is only marginally consistent with the XENON1T excess.

Figure 2 also summarizes terrestrial constraints, especially from CHARM-II, MiniBooNE, and NOMAD [33] (see section III D for details). These limits are most relevant for $M_N \gtrsim$ MeV. In this mass range, they strongly constrain the large-μ_ν parameter region. We emphasize that the limits from CHARM-II, MiniBooNE, and NOMAD are relevant only for transition magnetic moments between ν_μ and N_R. For ν_e–N_R and ν_τ–N_R couplings, these experiments do not set a constraint. In Figure 2 we also include Icecube sensitivity [35] as well as the region preferred by MiniBooNE data [32].

C. Borexino

XENON1T's constraints on neutrino magnetic moments are complemented by those based on neutrino–electron scattering in Borexino. We have recast the analysis performed by Borexino in ref. [20] for the low-energy recoil region. Analogously to XENON1T the expected differential event rate is given by eq. (9). The key differences are the increased number of target electrons $N_T = 3 \times 10^{31}$ and the detector efficiency, which for $E_r \in [200, 2600]$ keV is $\epsilon(E_r) \sim 1$. To determine the (Gaussian) energy resolution, we use the calibration data shown in fig. 21 of ref. [50], based on injecting monochromatic photons from the sources given in tab. II of the same reference. Borexino provides the full data underpinning fig. 2 of ref. [20] as well as a mapping between the number of PMT hits N_h and the recoil energy of the event in digital form [51]. We find a 5% mismatch between the given N_h–E_r mapping and the one obtained through fitting the calibration data in fig. 21 of ref. [50] in the region where the ^{7}Be and pep neutrino fluxes dominate. In our analysis, we correct for this mismatch by

correcting energies 5% upwards. We find that, with this corrections, our predictions for the solar neutrino event rates in the SM match Borexino's predictions very accurately.

To determine the 90% CL exclusion limit on the neutrino magnetic moment we perform a binned likelihood fit to the data from refs. [20, 51], similar to the fit to XENON1T data described in section II B above. For Borexino we allow the individual background components as well as the normalization of the various solar neutrino fluxes to vary. The best-fit point is very well consistent with $\mu_\nu = 0$. The exclusion contour shown in fig. 2 is obtained by assuming $\Delta\chi^2$ to follow a χ^2 distribution with two degrees of freedom. As a cross-check we compare our results to the constraint on a flavor-universal magnetic moment obtained in ref. [52]. We find $\mu_\nu < 3.1 \times 10^{-11} \, \mu_{\mathrm{B}}$ at 90% CL in this case, compared to $2.8 \times 10^{-11} \, \mu_{\mathrm{B}}$ in ref. [52]. Note that the constraint in fig. 2 is for couplings to muon neutrinos only, therefore the limit appearing in the figure is weaker.

There are two key differences between the electron recoil constraints from Borexino and XENON1T. First, at low M_N, XENON1T is more sensitive due its lower recoil energy threshold, which allows it to more efficiently probe the $1/E_r$-enhanced flux at low energies. Secondly, Borexino has greater sensitivity at larger M_N values due to the larger recoil energies measured in the detector, resulting in smaller E_ν^{min} cut-off values (see eq. (10)). Of course, also the larger size of Borexino plays an important role.

III. CONSTRAINTS

A. Stellar Cooling

1. Magnetic Moment Constraints from Stellar Cooling

Inside the hot plasma forming the core of a star, the dispersion relation of electromagnetic excitations (called plasmons) is modified in such a way that two-body decays into $\nu_L + N_R$, induced by the magnetic moment operator from eq. (1), can become kinematically allowed. For this to happen, it is required that N_R is lighter than the core temperature of the star. As ν_L and N_R can escape the star unhindered, they would constitute an efficient energy sink, greatly increasing the rate at which the star loses energy. Such excess energy loss, if too large, would be grossly inconsistent with our understanding of stellar evolution. Even under very conservative assumptions, tight limits on neutrino magnetic moments can thus be derived. For instance, to maintain its observed temperature in spite of the extra energy loss, the star would need to burn more fuel and would thus exhaust its fuel supply sooner. This way, limits on μ_ν can be derived from the simple fact that the Sun is still around after burning for 4.5 billion years. Stronger limits can be derived from a more detailed comparison to stellar evolution models

[53, 54]. As the core temperature of the Sun is of order keV, these limits extend up to right-handed neutrino masses of the same order. The reach in M_N can be extended by about an order of magnitude by looking at the evolution of red giant stars [41, 53, 55, 56]: at the tip of the red giant branch in the Hertzsprung–Russell diagram, where the helium flash occurs, the core temperature is on the order of $10\,\text{keV}$.

Starting from eq. (1), we compute the decay rate of transverse plasmons into $\nu + N_R$ in the comoving frame,

$$\Gamma_{\gamma^*} = \frac{|\mu_\nu|^2 K^4}{24\pi\,\omega}\left(1 - \frac{M_N^2}{K^2}\right)^2 \left(1 + 2\,\frac{M_N^2}{K^2}\right)\theta(K - M_N), \tag{14}$$

where $\theta(x)$ is the Heaviside step function, ω and k are the plasmon energy and momentum, respectively, and $K = \sqrt{\omega^2 - k^2}$ is the effective plasmon mass. The energy loss per unit volume is (see Appendix B of ref. [57])

$$Q = \int_0^\infty \frac{k^2 dk}{\pi^2} \int_{M_N^2}^\infty \frac{d\omega^2}{\pi} \frac{\omega\,\Gamma_T}{(K^2 - \omega_p^2)^2 + (\omega\Gamma_T)^2} \frac{\omega\,\Gamma_{\gamma^*}}{e^{\omega/T_\gamma} - 1}, \tag{15}$$

where $\Gamma_T = 8\pi\alpha^2 n_e/3m_e^2$ is the Thomson scattering rate. The plasma characteristics for a red-giant core just before helium ignition are taken from Table D.1 of ref. [53]. In particular, $\omega_p = 18\,\text{keV}$, $T_\gamma = 8.6\,\text{keV}$ and $n_e = 3 \times 10^{29}\,\text{cm}^{-3}$. We rely on the recent analysis of globular clusters in ref. [56], which sets an upper limit on the active neutrino magnetic moment $|\mu_\nu| < 2.2 \times 10^{-12}\,\mu_{\rm B}$. In order to recast this bound for the case of massive M_N, we equate the energy loss in eq. (15) for massive and massless N, and solve for the unknown $\mu_\nu(M_N)$. The obtained limits on μ_ν as a function of M_N are shown in fig. 2 as the purple exclusion region. For M_N smaller than the plasma frequency ω_p, the dominant effect comes from on-shell plasmon decays and the propagator in eq. (15) can effectively be approximated by the delta function $\propto \delta(K^2 - \omega_p^2)$. Instead, when $M_N > \omega_p$, the cooling process $\gamma + e^- \to e^- + N + \nu$ quickly becomes phase-space suppressed with increasing M_N.

2. Avoiding Stellar Cooling Constraints

Even though stellar cooling bounds are extremely robust, they are evaded in models in which the properties of the N_R depend dynamically on the surrounding matter density. Such "chameleon" models have been proposed originally to explain dark energy [58], but have also been invoked in other contexts, for instance to avoid stellar cooling constraints on axion-like particles [23, 59–64]. Consider a very light scalar field ϕ coupled to N_R through an operator of the form

$$\mathcal{L}_{\phi R} \supset \lambda_{\phi R}\phi\,\overline{N_R^c}N_R\,, \tag{16}$$

with a dimensionless coupling constant λ_ϕ. This operator implies that the N_R mass will be larger in environments of large N_R density such as the cores of stars. At the edge of the solar core (radius $0.1R_\odot$), the N_R mass shift due to the operator in eq. (16) will be of order

$$\Delta m_{RR} \sim 0.8\,\text{keV} \times \lambda_{\phi R}^2 \left(\frac{\text{meV}}{m_\phi}\right)^2 \left(\frac{n_R}{10^{11}\,\text{cm}^{-3}}\right) \tag{17}$$

for an N_R that would otherwise saturate the solar cooling bound. To arrive at this estimate, we have assumed that all emitted N_R have an energy of order $T_\odot \sim 1.5 \times 10^6$ Kelvin, that the total N_R luminosity equals the solar luminosity, and that the coupling λ_ϕ is of order one.

If ϕ couples not only to N_R, but also to SM quarks, the mass shift becomes proportional to the number density of SM fermions, which in the solar core ($\rho \simeq 150\,\text{grams/cm}^3$) is 15 orders of magnitude larger than the N_R number density that went into eq. (17), $n_{N_R} \simeq 10^{11}\,\text{cm}^{-3}$. On the other hand, ϕ couplings to SM fermions would typically proceed through mixing with the Higgs boson, which would lead to extra suppression by the small fermion Yukawa couplings and by the Higgs mixing angle θ, which is typically of order the mass ratio m_ϕ/m_H. Writing the ϕ coupling to quarks as $\mathcal{L}_{\phi q} \supset \sum_q \lambda_{\phi q}(\sqrt{2}m_q/v_H)(m_\phi/m_H)\,\phi\,\bar{q}q$, an additional contribution to the N_R mass of order

$$\Delta m_{Rq} \sim 0.008\,\text{keV} \times \lambda_{\phi R}\lambda_{\phi q}\left(\frac{\text{meV}}{m_\phi}\right)\left(\frac{m_q}{93\,\text{MeV}}\right) \tag{18}$$

ensues. To arrive at eq. (18), we have used the density of the solar core, $\rho_\odot = 150\,\text{grams/cm}^3$ [39], the SM Higgs mass $m_H = 125\,\text{GeV}$, and the SM Higgs vev $v_H = 246\,\text{GeV}$ [13]. For the quark content of the nucleon, $\sum_q m_q\,\langle\bar{q}q\rangle$, we have used the numbers from ref. [65]. We see that the mass shift due to the coupling to quarks will dominate for $m_\phi \gtrsim \text{eV}$ and for small $n_R \lesssim 1 \times 10^8\,\text{cm}^{-3}$. In these parameter regions, however, the magnitude of the shift is too small to evade stellar cooling constraints. For that, only the small-m_ϕ regime ($m_\phi \ll \text{eV}$) is interesting, where the contribution from eq. (18) can be safely neglected compared to the one from eq. (17).

B. Supernova 1987A

The reasoning that leads to stellar cooling constraints also applies to supernovae. The production of N_R through a magnetic moment operator would open up an efficient energy sink, which in turn would lead to faster cooling of the proto-neutron star [32, 53]. As a consequence, thermal emission of neutrinos would decline faster, and the duration of the observed neutrino burst would be shorter. Given that neutrinos from supernova 1987A were observed for about 10 seconds [66–68], bounds can be derived on the neutrino magnetic moment and on the mass of the right-handed neutrinos. The

corresponding exclusion region (dashed gray contour in fig. 2), taken from ref. [32], shows several characteristic features: obviously, very low $\mu_\nu \lesssim$ few $\times\, 10^{-13}\,\mu_{\rm B}$ cannot be constrained because the rate of N_R production is too small to be detectable in this case. However, the region with $\mu_\nu \gtrsim$ few $\times\, 10^{-10}\,\mu_{\rm B}$ cannot be constrained either. There, N_R interact too frequently to leave the supernova core, in spite of being copiously produced. Therefore, they do not contribute efficiently to the cooling of the core. Finally, the constraint peters out at $M_N \gtrsim 100\,{\rm MeV}$, where N_R are too heavy to be produced in plasmon decays.

While supernova constraints are part of the standard canon in studies of neutrino magnetic moments (and other manifestations of new physics at scales $\lesssim$ 100 MeV), they have recently been called into question [46]. The argument is that there is no evidence the neutrinos observed from SN 1987A were actually emitted from the core region of the exploding star. Rather, a hot accretion disk may have formed around a fast-rotating core, and the observed neutrino flux may have originated from this disk. As an accretion disk (unlike a supernova core) is optically thin not only to N_R, but also to ν_L, the production of N_R through a magnetic moment interaction would not lead to significant extra energy loss.

Even if the concerns raised in ref. [46] should be disproven with future observations, supernova constraints can still be relaxed by dedicated model-building along the lines of section III A 2. In particular, chameleon-like N_R, whose mass and/or couplings differ in the dense environment of a supernova core from those in vacuum can be invoked to prevent the production of N_R in supernovae, or to trap them inside to avoid excess cooling.

C. Cosmology

Just as in stars and supernovae, the magnetic moment operator from eq. (1) also opens a channel for producing N_R in the early Universe. For values of μ_ν large enough to be observable, N_R will always thermalize in the early Universe, unless the reheating temperature is extremely low. The main cosmological consequences of the resulting population of N_R are twofold:

- While N_R are relativistic, they contribute to the expansion rate, often parameterized in terms of the effective number of neutrino species, $N_{\rm eff}$.

- $N_R \to \nu_L + \gamma$ decays inject extra photons into the Universe.

$N_{\rm eff}$ is measured both at recombination and at the BBN epoch, with the CMB allowing a deviation of about 0.3 from the SM value $N_{\rm eff} = 3.045$ at 95% C.L. [69–71][1]

---

and BBN being even more restrictive ($N_{\rm eff} \lesssim 3.2$ at 95% C.L.) [74]. This implies that N_R should either never thermalize, or they should decay away before BBN, or they should decouple above the electroweak scale so that subsequent entropy production in the SM sector dilutes them sufficiently to satisfy these constraints. A naive estimate for the N_R decoupling temperature $T_{\rm dec}$ is obtained by equating the N_R production rate $\sim \alpha \mu_\nu^2 T^3$ to the Hubble rate $\sim T^2/M_{\rm Pl}$, where $M_{\rm Pl}$ is the Planck mass. This yields

$$T_{\rm dec} \simeq 1.28\,{\rm GeV} \times \left(\frac{10^{-11}\,\mu_{\rm B}}{\mu_\nu} \right)^2 . \qquad (19)$$

This shows that sufficiently early decoupling is only achieved if μ_ν is two to three orders of magnitude below the sensitivity of XENON1T.

From the N_R lifetime,

$$\begin{aligned} \tau_N &= \frac{16\pi}{\mu_\nu^2 M_N^3} \\ &= 3760\,{\rm sec} \times \left(\frac{1 \times 10^{-11}\,\mu_{\rm B}}{\mu_\nu} \right)^2 \left(\frac{\rm MeV}{M_N} \right)^3 , \end{aligned} \qquad (20)$$

we see that MeV-scale N_R will typically *not* decay before BBN. They will, however, decay before recombination if μ_ν is in the observable range. Therefore, the CMB is sensitive to μ_ν only through $N_{\rm eff}$, while the impact of a neutrino magnetic moment on BBN is more involved [75, 76]. We will now describe in detail how we derive BBN limits on neutrino transition magnetic moments.

1. Big Bang Nucleosynthesis

If N_R decays occur before the formation of heavy elements ($T \simeq 100\,{\rm keV}$), but after the freeze-out of weak interactions that can convert protons to neutrons ($T \simeq 1\,{\rm MeV}$), their main effect is through the modified expansion rate. Their presence in the Universe means that $p \leftrightarrow n$ interactions freeze out faster, leading to a larger neutron-to-proton ratio. Moreover, their decays alter the expansion and cooling rates and thus the time available for neutrons to decay and for BBN to proceed. If N_R decays happen after BBN, the extra photons from N_R decay decrease the baryon-to-photon ratio η. As η is precisely measured during recombination, this effect needs to be compensated by a larger η during BBN. Larger η renders deuterium disintegration less efficient. Once again, the presence of N_R before the onset of BBN implies that $p \leftrightarrow n$ reactions freeze out faster, and that neutrons have less time to decay. All three effects imply larger abundances of heavy elements.

To make these statements more quantitative, we have used a modified version [76] of the AlterBBN code [77, 78] that was kindly provided to us by Paul Frederik Depta, Marco Hufnagel, and Kai Schmidt-Hoberg, who developed it to constrain axion-like particles in ref. [76]. As input, this code requires a table listing the relation between

cosmological time t, the photon temperature T_γ, the neutrino temperature T_ν, the Hubble parameter H, and the photon number density. We obtain these quantities by solving the following set of (integrated) Boltzmann equations that describe the evolution of the photon, electron+positron, SM neutrino, and N_R energy densities ρ_γ, ρ_e, ρ_ν, and ρ_N:

$$
\begin{aligned}
\dot\rho_\gamma &= -4H\rho_\gamma + \langle\sigma v\rangle_{ee}(n_e\rho_e - n_e^{\rm eq}\rho_e^{\rm eq}) + \tfrac{1}{2}\Gamma_N(\rho_N - \rho_N^{\rm eq}), \\
\dot\rho_e &= -s_e H\rho_e - \langle\sigma v\rangle_{ee}(n_e\rho_e - n_e^{\rm eq}\rho_e^{\rm eq}), \\
\dot\rho_\nu &= -4H\rho_\nu + \tfrac{1}{2}\Gamma_N(\rho_N - \rho_N^{\rm eq}) + \Gamma_{eN}(\rho_N - \rho_N^{\rm eq}), \\
\dot\rho_N &= -s_N - \Gamma_N(\rho_N - \rho_N^{\rm eq}) - \Gamma_{eN}(\rho_N - \rho_N^{\rm eq}).
\end{aligned}
\tag{21}
$$

We now discuss the terms in these equations one by one. The first term in each equation describes dilution and redshifting due to Hubble expansion. For the massive species, this term includes a factor $s(m, T)$, which accounts for the transition from a relativistic to a non-relativistic species. It is given by

$$
s_i \equiv \frac{T}{\int dp\, f_i(m_i, T_i, p)} \int dp\, \frac{df_i(m_i, T_i, p)}{dT}, \tag{22}
$$

where $f_i(m_i, T_i, T_{i0}, p)$ is the phase space distribution function of species $i = e, N_R$. For electrons and positrons this is just the equilibrium distribution. For N_R, we use the equilibrium distribution while the rates of $N_R \leftrightarrow \gamma+\nu$ and $N_R+e \leftrightarrow \nu_L+e$ are larger than the Hubble rate. Otherwise, we use the distribution function for a species that has decoupled while still relativistic. As we will see that there are no parameter points at which N_R decouples while non-relativistic, this approximation is sufficient for our purposes.

In the terms describing e^+e^- annihilation in eq. (21), we approximate the annihilation cross section as $\langle\sigma v\rangle_{ee} \approx \min[\alpha^2/T_\gamma^2, \alpha^2 T_\gamma^2/(4m_e^4)]$, with α the electromagnetic fine structure constant and T_γ the photon temperature. This very rough approximation is sufficient to ensure that the e^+e^- energy density follows its equilibrium value,

$$
\rho_e^{\rm eq} = (2T_\gamma^4/\pi^2)J_f(m_e/T_\gamma), \tag{23}
$$

where $J_f(x)$ is a normalized integral over the Fermi-Dirac distribution:

$$
J_f(x) \equiv \int dy\, \frac{y^2\sqrt{x^2+y^2}}{\exp(\sqrt{x^2+y^2})+1}. \tag{24}
$$

The equilibrium number density n_e of electrons and positrons is defined in an analogous way as

$$
n_e^{\rm eq} = (2T_\gamma^3/\pi^2)I_f(m_e/T_\gamma), \tag{25}
$$

with

$$
I_f(x) \equiv \int dy\, \frac{y^2}{\exp(\sqrt{x^2+y^2})+1}. \tag{26}
$$

We calculate the actual number density, n_e from the energy density according to $n_e = \rho_e/T_\gamma \cdot I_f(m_e/T_\gamma)/J_f(m_e/T_\gamma)$.

There are two terms in eq. (21) that can alter the number density of N_R. The one containing $\Gamma_R = 1/\tau_R$ describes $N_R \to \gamma\nu$ decays and their inverse. This term contains the N_R equilibrium density $\rho_R^{\rm eq}$, which we compute in analogy to eq. (23), with the obvious replacement $m_e \to M_N$ and the perhaps not so obvious replacement $T_\gamma \to T_R = \tfrac{1}{2}(T_\nu + T_\gamma)$. Choosing this value for the N_R equilibrium temperature, we account for the fact that N_R decays to both neutrinos and photons. There is also a term describing the $2 \leftrightarrow 2$ process $e + N_R \leftrightarrow e + \nu_L$. We obtain the corresponding rate Γ_{eN} by computing the thermally averaged cross section $\langle\sigma v\rangle_{eN}$ and multiplying by n_e.

The treatment of the cosmological evolution outlined here is of course simplified – a more precise calculation would track not the integrated energy densities $\rho_{\gamma,e,\nu,R}$, but rather the individual phase space distribution functions. We have, however, verified that we can reproduce quite well the results of ref. [76] for the case of axion-like particles (ALPs), especially for the ^{4}He abundance. The latter is measured by the parameter $\mathcal{Y}_p \equiv \rho(^4{\rm He})/\rho_b$ which gives the ^{4}He mass fraction relative to the total baryonic mass density ρ_b. We have also verified that we correctly predict $N_{\rm eff} = 3.0$ in the SM at the CMB epoch. (The small correction to $N_{\rm eff}$ stemming from e^+e^- annihilation into neutrinos is ignored here as we will never use the absolute value of $N_{\rm eff}$, but only differences with respect to the SM.)

We plot our predictions for $\mathcal{Y}_p$ as a function of the right-handed neutrino mass and lifetime in fig. 3 (a). The corresponding constraint is also shown in fig. 2 as a red shaded region. Several different regimes are apparent, which can be understood given the arguments at the beginning of this section. At large mass and long lifetime, N_R decouple early, but remain abundant long after they have turned non-relativistic. The Universe thus enters a fully or partially matter-dominated phase, where it expands faster. Thus, $p \leftrightarrow n$ interactions freeze out faster and there is thus less time for neutrons to decay, implying larger abundances of the heavy elements. Moreover, when the N_R eventually decay, a large amount of energy is deposited in the photon and neutrino baths, decreasing the baryon-to-photon ratio η at recombination. To compensate, η must have been larger during BBN, rendering deuterium disintegration less efficient and once again contributing to larger abundances of the heavier elements. In the opposite limit of sub-MeV right-handed neutrinos, the N_R always decay after BBN. Once again, their presence during BBN implies a larger expansion rate, and their decays alter the baryon-to-photon ratio, leading to more efficient production of heavy elements. It is interesting that there is a sweet spot for MeV-scale N_R decoupling at a temperature of around $10\,{\rm GeV}$. In this case, the N_R decouple sufficiently early to be depleted by entropy production during the QCD phase transition,
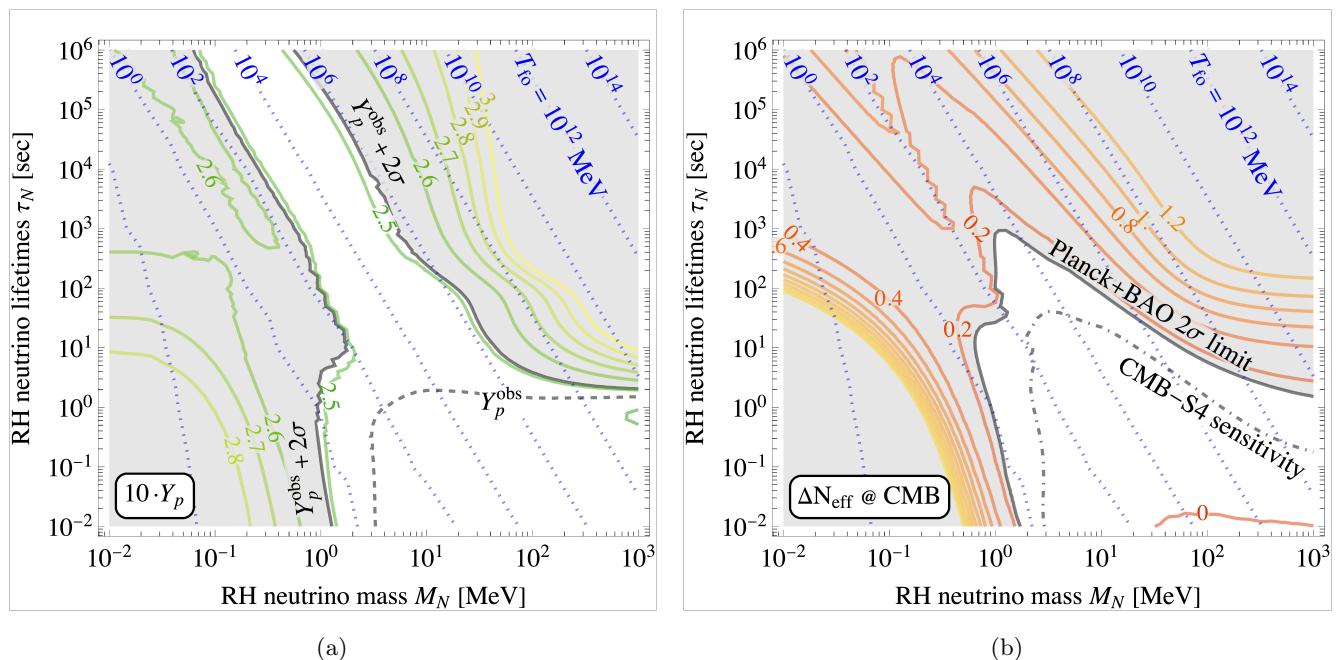
FIG. 3. (a) The predicted ^{4}He mass fraction $\mathcal{Y}_p \equiv \rho(^4\text{He})/\rho_b$ in the presence of right-handed neutrinos of mass M_N, decaying after a lifetime τ_N via $N_R \to \nu_L + \gamma$. The observational constraint $\mathcal{Y}_p = 0.245 \pm 0.006 \ (2\sigma)$ is taken from ref. [13]. We also show, as blue dotted contours, the temperature at which N_R freeze out from the thermal plasma (before recoupling later via $N_R \leftrightarrow \nu_L + \gamma$). The unsteady behavior in the upper left-hand part of the plot is due to numerical instability. (b) The predicted deviation of N_{eff}, the effective number of relativistic degrees of freedom at recombination, from the SM expectation. We use $N_{\text{eff}} = 2.90^{+0.30}_{-0.32} \ (2\sigma)$ for the current limit [47], and $N_{\text{eff}} = 3.045 \pm 0.06 \ (2\sigma)$ for the expected sensitivity of CMB-S4 [79]. The blue contours in this panel are the same as in panel (a).

while at the same time their mass is low enough to never dominate the energy density of the Universe.

It is important to note, though, that this sweet spot exists only for $\mathcal{Y}_p$. It is disfavored by the N_{eff} measurement at the CMB epoch (see fig. 3 (b) and discussion below in section III C 2), and also by the measured deuterium abundance. We do not include the latter in our suite of constraints because our predictions for this quantity are slightly less accurate than the ones for $\mathcal{Y}_p$ (as determined by comparing the results from our code to the ones from ref. [76] for the case of ALPs). We attribute this to the fact that we only track energy densities rather than full distribution functions.

We also do not consider the ^{3}He abundance, which would only lead to a very weak constraint in the upper right-hand corner of the M_N–τ_N plane. The ^{3}He abundance can be measured only locally, so its primordial abundance, which must be smaller than the local one, remains unknown.

2. Cosmic Microwave Background

Besides BBN, also the Cosmic Microwave Background (CMB) constrains the existence of N_R, in particular through the measurement of the effective number of degrees of relativistic degrees of freedom, N_{eff}. Our solution

to eq. (21) also yields a prediction for N_{eff} at the time of recombination. As we have made simplifications in our treatment of e^+e^- annihilation (in particular by neglecting Z-mediated annihilation to neutrinos), we consider only the difference ΔN_{eff} between the value of N_{eff} predicted by solving eq. (21) in the presence of non-zero μ_ν and the value $N_{\text{eff}} = 3.0$ predicted by these same equations in the SM. Our predictions for ΔN_{eff} are shown in fig. 3 (b), and the corresponding constraints are also included in fig. 2 as blue contours.

The qualitative behavior observed in fig. 3 (b) is similar to the one we have seen in fig. 3 (a). At large M_N and long lifetime, the Universe enters a phase of matter domination. The N_R eventually decay after neutrino decoupling, injecting half of the decay energy into the photon bath and the other half into neutrinos. As by that time the energy density of neutrinos is smaller by a factor $(4/11)^{4/3} \simeq 0.26$ than the energy density of photons, the relative impact onto the neutrinos is larger, thus N_{eff} increases. At low M_N and small τ_N, a rather interesting phenomenon occurs: As both the decay $N_R \leftrightarrow \gamma + \nu$ and the inelastic scattering process $N_R + e \leftrightarrow \nu + e$ remain in equilibrium for a very long time, they keep photons and neutrinos in equilibrium for much longer than in the SM. N_{eff} thus overshoots the SM value by a large amount. Between these two extremes, there is again a sweet spot where N_R decouple at about $T_{\text{dec}} \simeq 10\,\text{GeV}$, sufficiently

early to be substantially depleted during the QCD phase transition. At the same time, their mass is too low to compensate this depletion. Therefore, in this parameter region, the energy density of N_R never plays an important role during the evolution of the early Universe.

Besides setting a limit on N_{eff}, CMB observations also constrain neutrino magnetic moments in a more direct way. In particular, the CMB spectrum is sensitive to any extra energy injected at late times by N_R decays [80, 81]. However, fig. 5 in ref. [81] shows that the corresponding limits are always weaker than BBN constraints for N_R lifetimes $< 10^{12}$ sec. As lifetimes longer than this are outside the range of our plots, we will ignore these limits in the rest of this paper.

3. Avoiding Cosmological Constraints

Avoiding or weakening BBN and CMB constraints is not easy from a model-building point of view. One strategy is to prevent right-handed neutrino production in the early Universe altogether, for instance by coupling N_R to a scalar field φ whose vev evolves slowly over cosmological history [82, 83]. The corresponding operator $\lambda_\varphi \varphi \, \overline{N_R^c} N_R$ generates a dynamical contribution to the N_R mass. If $M_N \gg T$ in the early Universe, N_R production is forbidden and cosmological constraints are avoided.

Another possibility is the introduction of a second, invisible, decay mode for N_R which dominates over $N_R \to \nu_L + \gamma$. That way, injection of extra photons is avoided and only constraints on N_{eff} are relevant. As discussed above, these are satisfied if N_R decoupling is pushed to sufficiently early times, or if extra entropy is produced between N_R decoupling and BBN. One possibility for such an extra decay mode could be $N_R \to N_R' + \phi$, where N_R' is a second SM-singlet fermion and ϕ is a singlet scalar. Both N_R' and ϕ would need to be significantly lighter than M_N, and the coupling $\lambda_\phi \phi \bar{N}_R N_R'$ should be large. More precisely, the decay rate for $N_R \to N_R' + \phi$ is

$$\Gamma(N_R \to N_R' + \phi) = \frac{\lambda_\phi^2}{32\pi M_N^3}(M_N^2 + M_N'^2 - m_\phi^2)$$
$$\times \sqrt{(M_N^2 - M_N'^2 + m_\phi^2) - 4M_N^2 m_\phi^2}. \quad (27)$$

In the limit M_N', $m_\phi \to 0$, this becomes

$$\Gamma(N_R \to N_R' + \phi) \simeq 6.6 \times 10^{-20} \sec \times \lambda_\phi^2 \Big(\frac{M_N}{\text{MeV}}\Big). \quad (28)$$

That is, even for fairly small λ_ϕ, rapid decays can be realized. While a detailed study of such a scenario is beyond the scope of this work, qualitatively we see that if $M_N \gtrsim$ MeV, the N_R can be made to decay away before BBN becomes sensitive to their presence. For smaller M_N, at least the injection of extra photons can be avoided.

D. Terrestrial Constraints

While astrophysical and cosmological probes are particularly sensitive to relatively small neutrino magnetic moments, terrestrial experiments are essential for constraining parameter regions with large M_N and/or large μ_ν, where astrophysics and cosmology are often not sensitive. For large M_N, this is because the temperatures at which the constraining processes occur are too low to produce N_R. At large μ_ν, stellar cooling arguments are ineffective even for small M_N because N_R, while copiously produced in stars, would be trapped and therefore would not contribute significantly to stellar energy loss.

On Earth, N_R can be produced in beam dump experiments via upscattering of light neutrinos in the detector or close to it ($\nu_L + X_Z^A \to N_R + X_Z^A$), followed by the decay $N_R \to \nu_L + \gamma$ inside the fiducial volume. Moreover, N_R can be produced in meson decays close to the beam dump. In collider experiments, the main production channels are $e^+e^- \to N_R\nu_L$ (LEP), $\bar{q}q \to N_R\nu_L$, and $\bar{q}q' \to N_R\ell$ (LHC), where q, q' are SM quarks and ℓ is a SM lepton.

The terrestrial constraints shown in fig. 2 are taken from the compilation in ref. [33]. They are based on refs. [35, 84] for CHARM-II, on refs. [32, 85] for Mini-BooNE, and on refs. [35, 86] for NOMAD.

IV. ULTRA-VIOLET COMPLETION

In many ultraviolet (UV) extensions of the SM, transition magnetic moments between active and sterile neutrinos within the reach of direct dark matter detection experiments are disfavored or require severe fine-tuning. The reason is that large magnetic moments are often accompanied by prohibitively large contributions to the active neutrino masses. More precisely, when removing the photon line from the loop diagrams generating the magnetic moment, one typically obtains a contribution to the neutrino mass renormalization. In the following, we discuss the degree of fine-tuning required to circumvent this problem, and we show how tuning can be avoided in models with TeV-scale leptoquarks.

Neutrino masses and magnetic moments — Given that the loop diagrams generating active-to-sterile transition magnetic moments μ_ν and the ones inducing Dirac masses $m_{\nu N}$ are often closely related (see for instance fig. 4), a natural relation between μ_ν and $m_{\nu N}$ is given by

$$\frac{\mu_\nu}{\mu_B} \approx \frac{m_e \, m_{\nu N}}{\Lambda^2}, \quad (29)$$

where Λ is the mass scale of the UV completion. To recall, a Dirac mass term has the form $\mathcal{L} \supset m_{\nu N} \, \bar{\nu}_L N_R$, and the magnetic moment operator is $\mathcal{L} \supset \frac{1}{2}\mu_\nu \, \bar{\nu}_L \sigma_{\mu\nu} N_R \, F^{\mu\nu}$, see eq. (1). For new physics at the electroweak scale, and μ_ν within reach of XENON1T, the natural expectation

is $m_{\nu N} \gtrsim \mathcal{O}(\text{MeV})$. Only by allowing for tuning between $m_{\nu N}$ and other contributions to the active neutrino masses, the desired neutrino mass range $m_\nu \ll 1\,\text{eV}$ can be achieved. Additional contributions to neutrino masses can arise, for instance, from the type-I seesaw mechanism [87–90]. In this case, the generic expectation for the RH neutrino masses is $M_N \approx m_{\nu N}^2/m_\nu$, far above the mass range of interest to dark matter experiments. Tuning the tree-level Yukawa coupling $\mathcal{L}_Y \supset y_\nu \bar{L}_L \tilde{H} N_R$ such that the resulting tree-level contribution to the Dirac mass, $y_\nu v_H/\sqrt{2}$, nearly cancels the loop-induced contribution, the RH neutrino masses can be lowered to the MeV scale while keeping the active neutrino masses $m_\nu \ll \text{eV}$. As a side comment, note that the magnetic moment interaction also contributes to the Majorana mass term of ν_L at one-loop, see Fig. 3 in ref. [32]. This contribution is of order $\mu_\nu^2 \Lambda^2 M_N/(16\pi^2)$, so for the values of μ_ν and M_N that are of interest to XENON1T and Borexino, and for $\Lambda \sim \text{TeV}$, it is negligible.

In the inverse seesaw mechanism [91–93], lepton number conservation makes active neutrinos (almost) massless, while the sterile neutrino is a massive (pseudo) Dirac fermion. Thus, two gauge singlet Weyl fermions, N_L and N_R, are present. Gauge symmetry and lepton number conservation allow the mass terms $\mathcal{L} \supset -m_{\nu N} \bar{\nu}_L N_R - m_N \bar{N}_L N_R + \text{h.c.}$. The mixing $\tan\theta_{\nu N} = m_{\nu N}/m_N$ rotates gauge to mass eigenstates, predicting one massless chiral fermion and one massive Dirac fermion with mass $\sqrt{m_{\nu N}^2 + m_N^2}$. To obtain the observed non-zero masses for the active neutrinos, a small violation of lepton number is needed on top of this. Thus, the inverse seesaw mechanism can bring the sterile neutrino mass down to the range interesting for dark matter experiments without tuning, but at the expense of introducing a large active–sterile mixing angle, $\theta_{\nu N}$. The laboratory constraints on $\theta_{\nu N}$ from weak interactions depend on the sterile neutrino mass and the active flavor it mixes with. The limits are stronger for ν_e than for ν_μ and in particular ν_τ, but are still rather weak, requiring $m_{\nu N}$ to be about an order of magnitude below m_N for the relevant mass range [94–98]. Indeed, saturating the laboratory limits on the mixing angle is possible without terrible tuning of $m_{\nu N}$. However, keeping the mixing angle below cosmological limits while retaining a large neutrino magnetic moment again requires tuning of $m_{\nu N}$.

A leptoquark model — As a particular class of UV-complete theory featuring large μ_ν at one loop, let us consider models with TeV-scale leptoquark (LQs). We assume the dominant LQ coupling is with the third family of quarks, such that μ_ν does not suffer a large Yukawa suppression from the quark running in the loop. Another independent motivation to consider this setup comes from flavor physics. In particular, third generation leptoquarks are prime candidates for addressing the ongoing anomalies in B-meson decays [99–107]. A scalar leptoquark S_1 with $SU(3)_c \times SU(2)_L \times U(1)_Y$ quantum number $(\bar{\mathbf{3}}, \mathbf{1}, 1/3)$ is a prominent successful model pro-

posed in ref. [108]. The relevant Lagrangian is

$$\mathcal{L}_{S_1} \supset y_1\, \overline{b_R^{\,c}} N_R\, S_1 + y_2\, \overline{Q_L^3} L_L^{i\,c}\, S_1^\dagger + \text{h.c.}\,. \tag{30}$$

where Q_L^3, L_L^i, b_R, and N_R are a left-handed SM quark doublet of the third generation, a left-handed lepton doublet of flavor i, a right-handed bottom quark, and a right-handed neutrino, respectively, while the superscript c denotes a charge-conjugated field. Here, y_1 and y_2 are dimensionless Yukawa couplings. It is implied that the $SU(2)$ (anti)doublets ψ and χ are contracted with the two-dimensional Levi-Civita tensor, $\psi\chi \equiv \psi_1\chi_2 - \psi_2\chi_1$. The leading one-loop contribution to the ν_i–N_R transition neutrino magnetic moment is

$$\mu_\nu \approx \frac{e\, y_1 y_2}{8\pi^2 m_{LQ}^2}\, m_b \log\frac{m_b^2}{m_{LQ}^2}\,, \tag{31}$$

where m_b is the bottom mass, and m_{LQ} is the mass of the LQ. Thus, for $y_1 y_2 \approx 0.05$ and $m_{LQ} \approx 1\,\text{TeV}$, one obtains $|\mu_\nu| \approx 3 \times 10^{-11}\,\mu_B$, which is indeed within reach of XENON1T. Larger μ_ν would require larger Yukawa couplings; given the existing collider searches for leptoquarks at the LHC (discussed for instance in the recent review [109]), choosing m_{LQ} below a TeV is not an option.

In any case, as already pointed out, a sizeable contribution to the Dirac mass term $m_{\nu N}$ is generated by the diagrams in fig. 4 (with the photon line removed) and has to be tuned against the tree-level neutrino mass term.

Muon $g-2$ — Before we address this problem, let us first make a comparison with the charged-lepton magnetic moments, focusing on the muon case. The leptoquark interaction in eq. (30) will induce a contribution to the anomalous muon magnetic moment Δa_μ suppressed by the muon mass. For $m_{LQ} \sim 1\,\text{TeV}$ and $y_2 \sim 1$, the contribution to Δa_μ is about an order of magnitude smaller than the observed discrepancy between the theoretical prediction and the measurement by the E821 experiment at BNL [110]. In other words, in this model, neutrino transition magnetic moments observable in XENON1T are not in conflict with measurements from the charged-lepton sector. In fact, the current anomaly in muon $g-2$ can be fully accommodated if additional interactions are present. The S_1 leptoquark has another independent gauge invariant interaction, $\mathcal{L} \supset y_1'\, \overline{t_R^{\,c}} e_R^i\, S_1$, with the right-handed top quark and a charged lepton. Even a small coupling, $y_1' \sim 10^{-3}$ is enough to accommodated Δa_μ, owing to the chiral enhancement from the top quark in the loop [111]. The corresponding one-loop correction to the muon mass in this case is below the tree-level one. In passing we note that an alternative muon $g-2$ explanation with leptoquarks was studied in [112] (see also recent Ref. [113]).

Voloshin mechanism with leptoquarks — We now review a mechanism for breaking the relation eq. (29) between neutrino magnetic moments and neutrino masses,
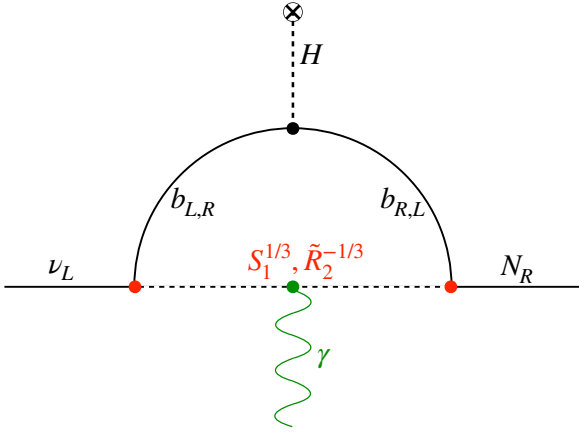
FIG. 4. The one-loop contribution to the neutrino magnetic moment induced by eqs. (30) and (32). Note that both $S_1^{1/3}$ and $\tilde{R}_2^{-1/3}$ can run in the loop. If the photon line is removed, these diagrams also contribute to neutrino masses. Combining $S_1^{1/3}$ and $\tilde{R}_2^{-1/3}$ into a doublet under a horizontal $SU(2)_H$ symmetry, their one-loop contributions to neutrino masses cancel exactly, while no cancellation occurs for the magnetic moment.

and we implement this mechanism in the context of TeV-scale leptoquarks. The basic observation is that, due to the Lorentz structure of the defining operators, the neutrino mass matrix is symmetric while the magnetic moment matrix is antisymmetric in flavor space. This feature is exploited by the Voloshin mechanism for one-loop models [114]. Voloshin postulated an approximate global $SU(2)_H$ symmetry, under which (ν_L^c, N_R) transforms as a doublet, thus allowing the magnetic moment term $\bar{N}_R \sigma^{\mu\nu} \nu_L - \overline{\nu_L^c} \sigma^{\mu\nu} N_R^c$, which is an $SU(2)_H$ singlet, while forbidding the $SU(2)_H$ triplet mass term $\bar{N}_R \nu_L + \overline{\nu_L^c} N_R^c$.

To realize this mechanism in the leptoquark scenario, we add in addition to S_1 a second leptoquark $\tilde{R}_2 \equiv (\mathbf{3}, \mathbf{2}, 1/6)$, with interactions

$$\mathcal{L}_{\tilde{R}_2} \supset -y_1 \, \tilde{R}_2^\dagger \, \overline{b_R^c} L_L^{ic} + y_2 \, \overline{Q_L^3} N_R \, \tilde{R}_2 + \text{h.c.}. \qquad (32)$$

Note that $\mathcal{L} \supset \mathcal{L}_{\tilde{R}_2} + \mathcal{L}_{S_1}$ respects the global $SU(2)_H$ symmetry under which $(\tilde{R}_2^{-1/3}, S_1^\dagger)$ and (ν_L^c, N_R) transform as doublets. The $SU(2)_H$ symmetry of this sector is preserved by QCD and QED, but is explicitly broken by $SU(2)_L \times U(1)_Y$ gauge interactions and by the lepton Yukawa couplings. In the limit of an exact $SU(2)_H$, the Dirac mass term $m_{\nu N}$ is exactly zero, while a transition magnetic moment is generated. In other words, the two diagrams fig. 4 (without the photon) cancel exactly since the $SU(2)_H$ symmetry requires the leptoquarks to be mass-degenerate, and the product of the couplings in the red vertices to be equal and opposite in the two diagrams. For the neutrino magnetic moment (fig. 4 with the photon included), the relative sign between the two contributing diagrams is flipped thanks to the opposite electric charges of the particles to which the photon line

is attached. Note that $SU(2)_H$ encompasses lepton number, thus the leptoquark loops will not generate a Majorana mass term for neutrinos.

There are several terms in the Lagrangian that explicitly break $SU(2)_H$ symmetry:

1. The charged lepton Yukawa couplings. This source of $SU(2)_H$ breaking is small thanks to the smallness of the charged lepton masses.

2. Electroweak radiative corrections. These terms, related to the different $SU(2)_L \times U(1)_Y$ quantum numbers within the $SU(2)_H$ multiplets, are somewhat more important. Radiative corrections are still suppressed by $\alpha/(4\pi)$, so while they do generate a neutrino Dirac mass $m_{\nu N}$, it is suppressed by more than three orders of magnitude compared to its value in leptoquark models without the Voloshin mechanism. In other words, the cancellation of the diagrams in fig. 4 is still spoiled, but only at the two-loop level.

3. The Majorana mass term for the right-handed neutrino, which breaks not only $SU(2)_H$, but also lepton number, thus feeding into the active neutrino masses by the type-I seesaw formula.

In spite of these $SU(2)_H$ breaking terms, even for an MeV-scale right-handed neutrino only a mild cancellation between the loop-induced and tree level mass terms is needed to obtain the correct active neutrino mass scale and to sufficiently suppress the mixing angle. If somewhat more fine-tuning is accepted, it is also possible to generate active neutrino masses predominantly through yet another $SU(2)_H$ breaking source, namely by introducing an independent term $(\bar{L}_L \tilde{H})(\tilde{H}^T L_L^c)$. Finally, if the inverse seesaw mechanism is invoked, neutrino masses and mixing angles can be completely decoupled.

B**-meson anomalies** — To connect the discussion to far to various hints for lepton flavor universality violation in B-decays, note that these hints can be explained by a scalar leptoquark with SM quantum numbers $(\bar{\mathbf{3}}, \mathbf{1}, 1/3)$, coupled predominantly to third generation quarks [99–107]. This is precisely our S_1 leptoquark. In fact, the S_1 leptoquark can act as a mediator both in neutral current transitions, $b \to s\ell^+\ell^-$, and in charged current transitions, $b \to c\tau\nu$. Here we discuss the two cases separately.

The charged current anomaly in

$$R(D^{(*)}) \equiv \frac{\text{BR}(B \to D^{(*)}\tau\nu)}{\text{BR}(B \to D^{(*)}\mu\nu)} \qquad (33)$$

requires leptoquark couplings to tau leptons ($i = 3$ in eq. (30)), implying a connection with the ν_τ transition magnetic moment. The effect on $R(D^{(*)})$ is generated by tree-level leptoquark exchange between the quark and lepton currents. Two different scenarios are possible depending on the neutrino into which the B-meson decays. If in eq. (30) one imposes $y_1 \ll y_2$, decays into ν_τ will dominate, as suggested in refs. [108, 115]. The

preferred parameter range is roughly $m_{LQ} \sim \mathcal{O}(\text{TeV})$ and $y_2 \sim \mathcal{O}(1)$. In the other scenario, the coupling y_1 in eq. (30) dominates, so the B-meson decays into the sterile neutrino N_R, see refs. [116, 117]. Interestingly enough, the parameter range of interest for both, B-decays and the neutrino magnetic moment, has a sizeable overlap.

The neutral current anomaly in the ratio

$$R(K^{(*)}) \equiv \frac{\text{BR}(B \to K^{(*)}\mu^+\mu^-)}{\text{BR}(B \to K^{(*)}e^+e^-)}\bigg|_{q^2_{\min} < q^2 < q^2_{\max}} , \quad (34)$$

requires a leptoquark coupling to muons or electrons ($i = 2$ or $i = 1$ in eq. (30)), implying a connection with ν_μ or ν_e transition magnetic moment. In refs. [108, 115, 118, 119], the dominant effect in $b \to s\mu^+\mu^-$ transitions comes from a box diagram at one-loop induced by the y_2 coupling from eq. (30). Interestingly, the anomalies are again explained for $m_{LQ} \sim \mathcal{O}(\text{TeV})$ and $y_2 \sim \mathcal{O}(1)$, the same parameter range required to generate a sizeable neutrino magnetic moment. Note that the additional presence of the $\tilde{R}_2$ leptoquark does not give corrections to $R(K^{(*)})$ if only the interactions in eq. (32) are present. Another direction to be explored is to utilize $\tilde{R}_2$ at tree-level, introducing a small leptoquark coupling with the right-handed strange quark, as done for example in ref. [120]. A detailed analysis of flavor physics constraints on the generation of neutrino magnetic moments is left for future work.

Magnetic moment $\nu_e \to \nu_\mu$ with leptoquarks — Let us finally discuss how transition magnetic moments among the active neutrinos can be generated in models without heavier sterile states. In most models, this requires severe tuning to avoid too large neutrino masses. As shown in ref. [121, 122], operator mixing under renormalization sets a stringent naturalness bound for active neutrinos of Dirac type. This bound is avoided in the case of transition magnetic moments if the active neutrinos are Majorana [123, 124]. One interesting model generating a transition magnetic moment $\mu_{\nu_e\nu_\mu}$ between the ν_e and ν_μ flavors without undue tuning was recently proposed in ref. [17]. In this model, $SU(2)_H$ symmetry is not explicitly broken by gauge interactions – the colorless scalars $\eta^a \equiv (\mathbf{1}, \mathbf{1}, 1)$ and $\Phi^a \equiv (\mathbf{1}, \mathbf{2}, 1/2)$ come in two copies ($a = 1, 2$) as $SU(2)_H$ doublets, separately. The required η–Φ mass mixing is introduced via the Higgs mechanism. This model therefore has less $SU(2)_H$ breaking and thus more effectively protects the small neutrino masses. Since there are no N_R states in ref. [17], active–sterile mixing is not a concern either. Interestingly, the leading $SU(2)_H$ breaking due to the muon Yukawa coupling elegantly generates the correct neutrino mass scale. We would like to point out that the same can be achieved with our leptoquarks. Let S_1^a and $\tilde{R}_2^a$ ($a = 1, 2$) both be doublets of $SU(2)_H$. Their mass mixing is given by the lepton number violating operator $H^\dagger \tilde{R}_2^a \epsilon^{ab} S_1^b$, while the role of the τ lepton in ref. [17] is replaced by the bottom quark. More precisely, the y_2 interaction in eq. (30) and the y_1 interaction in eq. (32) are invariant under $SU(2)_H$ when (L_e, L_μ) are combined into an $SU(2)_H$ doublet.

This is an alternative to the model of ref. [17] for simultaneously realizing small neutrino masses and large $\mu_{\nu_e\nu_\mu}$, with quite different collider and flavor phenomenology worth exploring.

To complete the discussion, we note that the leptoquark model for $\mu_{\nu_e\nu_\mu}$ can be embedded in the context of RPV SUSY, see refs. [125, 126] for an early work in this direction. Also, for recent studies on the neutrino mass generation with S_1 and $\tilde{R}_2$ see refs. [127–130].

V. CONCLUSIONS

In summary, we have discussed neutrino magnetic moments in a broad context, highlighting in particular the following take-home messages:

1. While most of the existing literature on this topic is focused on magnetic moments coupling sub-eV states, transition magnetic moments with right-handed neutrinos at larger mass are equally well motivated, and offer a much richer phenomenology.

2. Direct dark matter searches offer superb sensitivity to neutrino magnetic moments. Our analysis of XENON1T data sets some of the strongest limits on the parameter space spanned by the magnetic moment μ_ν and the RH neutrino mass M_N.

3. A transition magnetic moments of order $\mu_\nu \simeq 6 \times 10^{-11} \mu_{\rm B}$ (for coupling to muon neutrinos only) with a RH neutrino mass $M_N \simeq 100\,{\rm keV}$ might explain the XENON1T anomaly if conservative assumptions are adopted for the SN1987A and CMB $N_{\rm eff}$ limits.

4. Strong constraints on the parameter space are imposed by stellar cooling and BBN. We have carried out in particular a detailed study of the latter. Other cosmological constraints, which might spoil the explanation of the XENON1T anomaly, are less robust: the limit from SN1987A is avoided if the neutrino flux from this supernova was dominated by accretion onto the supernova core rather than cooling of the core itself [46]. The CMB measurement of $N_{\rm eff}$ needs to be taken with a grain of salt in view of the persisting H_0 tension, which prefers $N_{\rm eff} > 3$.

5. Neutrino magnetic moments and neutrino masses, both manifestations of chirality-flipping interactions, are typically interlinked in a high-energy theory. Thus, large magnetic moments are difficult to reconcile with the observed smallness of neutrino masses. This conclusion can, however, be avoided, as we have illustrated in a TeV-scale leptoquark model that has been recently proposed as a solution to B-physics anomalies and the muon $g - 2$ anomaly. We have implemented the Voloshin mechanism [114] in this model by postulating that the

two leptoquarks appearing in it are members of a doublet under an approximate $SU(2)_H$ horizontal symmetry. As a result, the phenomenology of the right-handed neutrinos is dominated by the transition magnetic moment rather than the active–sterile mixing, as commonly assumed in the literature.

Most of our results are concisely summarized in fig. 2, which collects the various constraints on neutrino magnetic moments that we have discussed.

We believe that because of their rich phenomenology and manifold connections to other areas of particle physics, astrophysics, and cosmology, neutrino transition magnetic moments are a prime target for current and future direct dark matter searches, given that these detectors will be able to set the most stringent terrestrial limits. Using these detectors in that way highlights once more that running modern underground experiments does not mean sitting next to a tank of liquid and waiting, as some critics have claimed in the past. Rather, it means operating a multi-purpose observatory with a rich and diverse physics program, and with results that will reverberate throughout many domains of fundamental physics for years to come.

[1] M. W. Goodman and E. Witten, *Detectability of Certain Dark Matter Candidates*, *Phys. Rev.* **D31** (1985) 3059.

[2] A. Drukier and L. Stodolsky, *Principles and Applications of a Neutral Current Detector for Neutrino Physics and Astronomy*, *Phys. Rev.* **D30** (1984) 2295.

[3] A. Gutlein *et al.*, *Solar and atmospheric neutrinos: Background sources for the direct dark matter search*, *Astropart. Phys.* **34** (2010) 90–96, [1003.5530].

[4] R. Harnik, J. Kopp, and P. A. N. Machado, *Exploring nu Signals in Dark Matter Detectors*, *JCAP* **1207** (2012) 026, [1202.6073].

[5] J. L. Feng *et al.*, *Planning the Future of U.S. Particle Physics (Snowmass 2013): Chapter 4: Cosmic Frontier*, in *Proceedings, 2013 Community Summer Study on the Future of U.S. Particle Physics: Snowmass on the Mississippi (CSS2013): Minneapolis, MN, USA, July 29-August 6, 2013*, 2014. 1401.6085.

[6] K. Fujikawa and R. Shrock, *The Magnetic Moment of a Massive Neutrino and Neutrino Spin Rotation*, *Phys. Rev. Lett.* **45** (1980) 963.

[7] B. W. Lee and R. E. Shrock, *Natural Suppression of Symmetry Violation in Gauge Theories: Muon - Lepton and Electron Lepton Number Nonconservation*, *Phys. Rev. D* **16** (1977) 1444.

[8] S. T. Petcov, *The Processes $\mu \to e + \gamma$, $\mu \to e + e + \bar{e}$, $\nu' \to \nu + \gamma$ in the Weinberg-Salam Model with Neutrino Mixing*, *Sov. J. Nucl. Phys.* **25** (1977) 340. [Yad. Fiz.25,641(1977); Erratum: Sov. J. Nucl. Phys.25,698(1977); Erratum: Yad. Fiz.25,1336(1977)].

[9] P. B. Pal and L. Wolfenstein, *Radiative Decays of Massive Neutrinos*, *Phys. Rev.* **D25** (1982) 766.

[10] R. E. Shrock, *Electromagnetic Properties and Decays of Dirac and Majorana Neutrinos in a General Class of Gauge Theories*, *Nucl. Phys.* **B206** (1982) 359–379.

[11] M. Dvornikov and A. Studenikin, *Electric charge and magnetic moment of massive neutrino*, *Phys. Rev.* **D69** (2004) 073001, [hep-ph/0305206].

[12] C. Giunti and A. Studenikin, *Neutrino electromagnetic interactions: a window to new physics*, *Rev. Mod. Phys.* **87** (2015) 531, [1403.6344].

[13] **Particle Data Group Collaboration**, M. Tanabashi *et al.*, *Review of Particle Physics*, *Phys. Rev.* **D98** (2018), no. 3 030001.

[14] R. Shrock, *Decay $l_0 \to \nu$ (lepton) γ in gauge theories of weak and electromagnetic interactions*, *Phys. Rev. D* **9** (1974) 743–748.

[15] M. Fukugita and T. Yanagida, *Physics of neutrinos and applications to astrophysics*. 2003.

[16] M. Lindner, B. Radovčić, and J. Welter, *Revisiting Large Neutrino Magnetic Moments*, *JHEP* **07** (2017) 139, [1706.02555].

[17] K. S. Babu, S. Jana, and M. Lindner, *Large Neutrino Magnetic Moments in the Light of Recent Experiments*, 2007.04291.

[18] X.-J. Xu, *Tensor and scalar interactions of neutrinos may lead to observable neutrino magnetic moments*, *Phys. Rev. D* **99** (2019), no. 7 075003, [1901.00482].

[19] **XENON Collaboration**, E. Aprile *et al.*, *Observation of Excess Electronic Recoil Events in XENON1T*, 2006.09721.

[20] **BOREXINO Collaboration**, M. Agostini *et al.*, *Comprehensive measurement of pp-chain solar neutrinos*, *Nature* **562** (2018), no. 7728 505–510.

[21] I. M. Shoemaker, Y.-D. Tsai, and J. Wyenberg, *An Active-to-Sterile Neutrino Transition Dipole Moment*

and the XENON1T Excess, 2007.05513.

[22] H. An, M. Pospelov, J. Pradler, and A. Ritz, *New limits on dark photons from solar emission and keV scale dark matter*, 2006.13929.

[23] I. M. Bloch, A. Caputo, R. Essig, D. Redigolo, M. Sholapurkar, and T. Volansky, *Exploring New Physics with O(keV) Electron Recoils in Direct Detection Experiments*, 2006.14521.

[24] N. Okada, S. Okada, D. Raut, and Q. Shafi, *Dark Matter Z' and XENON1T Excess from $U(1)_X$ Extended Standard Model*, 2007.02898.

[25] N. F. Bell, J. B. Dent, B. Dutta, S. Ghosh, J. Kumar, and J. L. Newstead, *Explaining the XENON1T excess with Luminous Dark Matter*, 2006.12461.

[26] J. Bramante and N. Song, *Electric But Not Eclectic: Thermal Relic Dark Matter for the XENON1T Excess*, 2006.14089.

[27] D. Choudhury, S. Maharana, D. Sachdeva, and V. Sahdev, *Dark Matter, Muon Anomalous Magnetic Moment and the XENON1T Excess*, 2007.08205.

[28] Y. Farzan and M. Rajaee, *Pico-charged particles explaining 511 keV line and XENON1T signal*, 2007.14421.

[29] L. Di Luzio, M. Fedele, M. Giannotti, F. Mescia, and E. Nardi, *Solar axions cannot explain the XENON1T excess*, 2006.12487.

[30] C. Gao, J. Liu, L.-T. Wang, X.-P. Wang, W. Xue, and Y.-M. Zhong, *Re-examining the Solar Axion Explanation for the XENON1T Excess*, 2006.14598.

[31] P. Vogel and J. Engel, *Neutrino Electromagnetic Form-Factors*, *Phys. Rev.* **D39** (1989) 3378.

[32] G. Magill, R. Plestid, M. Pospelov, and Y.-D. Tsai, *Dipole Portal to Heavy Neutral Leptons*, *Phys. Rev.* **D98** (2018), no. 11 115015, [1803.03262].

[33] I. M. Shoemaker and J. Wyenberg, *Direct Detection Experiments at the Neutrino Dipole Portal Frontier*, *Phys. Rev. D* **99** (2019), no. 7 075010, [1811.12435].

[34] A. Balantekin and N. Vassh, *Magnetic moments of active and sterile neutrinos*, *Phys. Rev. D* **89** (2014), no. 7 073013, [1312.6858].

[35] P. Coloma, P. A. Machado, I. Martinez-Soler, and I. M. Shoemaker, *Double-Cascade Events from New Physics in Icecube*, *Phys. Rev. Lett.* **119** (2017), no. 20 201804, [1707.08573].

[36] J. Engel, *Nuclear form-factors for the scattering of weakly interacting massive particles*, *Phys. Lett.* **B264** (1991) 114–119.

[37] M. Lindner, W. Rodejohann, and X.-J. Xu, *Coherent Neutrino-Nucleus Scattering and new Neutrino Interactions*, *JHEP* **03** (2017) 097, [1612.04150].

[38] V. A. Bednyakov and D. V. Naumov, *Coherency and incoherency in neutrino-nucleus elastic and inelastic scattering*, *Phys. Rev. D* **98** (2018), no. 5 053004, [1806.08768].

[39] J. N. Bahcall, A. M. Serenelli, and S. Basu, *New solar opacities, abundances, helioseismology, and neutrino fluxes*, *Astrophys. J. Lett.* **621** (2005) L85–L88, [astro-ph/0412440].

[40] E. K. Akhmedov, *Neutrino physics*, hep-ph/0001264.

[41] S. Arceo-Díaz, K.-P. Schröder, K. Zuber, and D. Jack, *Constraint on the magnetic dipole moment of neutrinos by the tip-RGB luminosity in ω -Centauri*, *Astropart. Phys.* **70** (2015) 1–11.

[42] **XENON Collaboration**, E. Aprile *et al.*, *Dark Matter Search Results from a One Ton-Year Exposure of XENON1T*, *Phys. Rev. Lett.* **121** (2018), no. 11 111302, [1805.12562].

[43] **XENON Collaboration**, E. Aprile *et al.*, *Observation of two-neutrino double electron capture in ^{124}Xe with XENON1T*, *Nature* **568** (2019), no. 7753 532–535, [1904.11002].

[44] **XENON100 Collaboration**, E. Aprile *et al.*, *The neutron background of the XENON100 dark matter search experiment*, *J. Phys. G* **40** (2013) 115201, [1306.2303].

[45] **DARWIN Collaboration**, J. Aalbers *et al.*, *DARWIN: towards the ultimate dark matter detector*, *JCAP* **11** (2016) 017, [1606.07001].

[46] N. Bar, K. Blum, and G. D'amico, *Is there a supernova bound on axions?*, *Phys. Rev.* **D101** (2020) 123025, [1907.05020].

[47] O. H. Philcox, M. M. Ivanov, M. Simonović, and M. Zaldarriaga, *Combining Full-Shape and BAO Analyses of Galaxy Power Spectra: A 1.6% CMB-independent constraint on H0*, *JCAP* **05** (2020) 032, [2002.04035].

[48] J. L. Bernal, L. Verde, and A. G. Riess, *The trouble with H_0*, *JCAP* **10** (2016) 019, [1607.05617].

[49] L. Knox and M. Millea, *Hubble constant hunter's guide*, *Phys. Rev. D* **101** (2020), no. 4 043533, [1908.03663].

[50] **Borexino Collaboration**, M. Agostini *et al.*, *The Monte Carlo simulation of the Borexino detector*, *Astropart. Phys.* **97** (2018) 136–159, [1704.02291].

[51] **Borexino Collaboration**, 2020. online data repository at https://bxopen.lngs.infn.it/.

[52] **Borexino Collaboration**, M. Agostini *et al.*, *Limiting neutrino magnetic moments with Borexino Phase-II solar neutrino data*, *Phys. Rev. D* **96** (2017), no. 9 091103, [1707.09355].

[53] G. G. Raffelt, *Stars as laboratories for fundamental physics*. 1996.

[54] G. Raffelt, *Limits on neutrino electromagnetic properties: An update*, *Phys. Rept.* **320** (1999) 319–327.

[55] G. Raffelt and A. Weiss, *Red giant bound on the axion - electron coupling revisited*, *Phys. Rev. D* **51** (1995) 1495–1498, [hep-ph/9410205].

[56] S. A. Díaz, K.-P. Schröder, K. Zuber, D. Jack, and E. E. B. Barrios, *Constraint on the axion-electron coupling constant and the neutrino magnetic dipole moment by using the tip-RGB luminosity of fifty globular clusters*, 1910.10568.

[57] H. Vogel and J. Redondo, *Dark Radiation constraints on minicharged particles in models with a hidden photon*, *JCAP* **02** (2014) 029, [1311.2600].

[58] J. Khoury and A. Weltman, *Chameleon cosmology*, *Phys. Rev.* **D69** (2004) 044026, [astro-ph/0309411].

[59] E. Masso and J. Redondo, *Evading astrophysical constraints on axion-like particles*, *JCAP* **0509** (2005) 015, [hep-ph/0504202].

[60] J. Jaeckel, E. Masso, J. Redondo, A. Ringwald, and F. Takahashi, *The Need for purely laboratory-based axion-like particle searches*, *Phys. Rev.* **D75** (2007) 013004, [hep-ph/0610203].

[61] A. K. Ganguly, P. Jain, S. Mandal, and S. Stokes, *Self Interacting Dark Matter in the Solar System*, *Phys. Rev.* **D76** (2007) 025026, [hep-ph/0611006].

[62] J. E. Kim, *PVLAS experiment, star cooling and BBN constraints: Possible interpretation with temperature dependent gauge symmetry breaking*, *Phys. Rev.* **D76** (2007) 051701, [0704.3310].

[63] P. Brax, C. van de Bruck, and A.-C. Davis, *Compatibility of the chameleon-field model with fifth-force experiments, cosmology, and PVLAS and CAST results*, *Phys. Rev. Lett.* **99** (2007) 121103, [hep-ph/0703243].

[64] J. Redondo, *Can the PVLAS particle be compatible with the astrophysical bounds?* PhD thesis, Barcelona, Autonoma U., 2007. 0807.4329.

[65] **RQCD Collaboration**, G. S. Bali, S. Collins, D. Richtmann, A. Schäfer, W. Söldner, and A. Sternbeck, *Direct determinations of the nucleon and pion σ terms at nearly physical quark masses*, *Phys. Rev.* **D93** (2016), no. 9 094504, [1603.00827].

[66] **Kamiokande-II Collaboration**, K. Hirata *et al.*, *Observation of a Neutrino Burst from the Supernova SN 1987a*, *Phys. Rev. Lett.* **58** (1987) 1490–1493.

[67] E. N. Alekseev, L. N. Alekseeva, I. V. Krivosheina, and V. I. Volchenko, *Detection of the Neutrino Signal From SN1987A in the LMC Using the Inr Baksan Underground Scintillation Telescope*, *Phys. Lett.* **B205** (1988) 209–214.

[68] R. M. Bionta *et al.*, *Observation of a Neutrino Burst in Coincidence with Supernova SN 1987a in the Large Magellanic Cloud*, *Phys. Rev. Lett.* **58** (1987) 1494.

[69] **Planck Collaboration**, N. Aghanim *et al.*, *Planck 2018 results. VI. Cosmological parameters*, 1807.06209.

[70] P. F. de Salas and S. Pastor, *Relic neutrino decoupling with flavour oscillations revisited*, *JCAP* **1607** (2016) 051, [1606.06986].

[71] K. Akita and M. Yamaguchi, *A precision calculation of relic neutrino decoupling*, 2005.07047.

[72] M. Escudero, *Neutrino decoupling beyond the Standard Model: CMB constraints on the Dark Matter mass with a fast and precise $N_{\rm eff}$ evaluation*, *JCAP* **02** (2019) 007, [1812.05605].

[73] M. Escudero Abenza, *Precision Early Universe Thermodynamics made simple: $N_{\rm eff}$ and Neutrino Decoupling in the Standard Model and beyond*, *JCAP* **05** (2020) 048, [2001.04466].

[74] R. H. Cyburt, B. D. Fields, K. A. Olive, and T.-H. Yeh, *Big Bang Nucleosynthesis: 2015*, *Rev. Mod. Phys.* **88** (2016) 015004, [1505.01076].

[75] D. Cadamuro and J. Redondo, *Cosmological bounds on pseudo Nambu-Goldstone bosons*, *JCAP* **1202** (2012) 032, [1110.2895].

[76] P. F. Depta, M. Hufnagel, and K. Schmidt-Hoberg, *Robust cosmological constraints on axion-like particles*, *JCAP* **05** (2020) 009, [2002.08370].

[77] A. Arbey, *AlterBBN: A program for calculating the BBN abundances of the elements in alternative cosmologies*, *Comput. Phys. Commun.* **183** (2012) 1822–1831, [1106.1363].

[78] A. Arbey, J. Auffinger, K. Hickerson, and E. Jenssen, *AlterBBN v2: A public code for calculating Big-Bang nucleosynthesis constraints in alternative cosmologies*, *Comput. Phys. Commun.* **248** (2020) 106982, [1806.11095].

[79] **CMB-S4 Collaboration**, K. N. Abazajian *et al.*, *CMB-S4 Science Book, First Edition*, 1610.02743.

[80] T. R. Slatyer and C.-L. Wu, *General Constraints on Dark Matter Decay from the Cosmic Microwave Background*, *Phys. Rev. D* **95** (2017), no. 2 023010, [1610.06933].

[81] V. Poulin, J. Lesgourgues, and P. D. Serpico, *Cosmological constraints on exotic injection of electromagnetic energy*, *JCAP* **03** (2017) 043, [1610.10051].

[82] F. Bezrukov, A. Chudaykin, and D. Gorbunov, *Hiding an elephant: heavy sterile neutrino with large mixing angle does not contradict cosmology*, *JCAP* **1706** (2017) 051, [1705.02184].

[83] Y. Farzan, *Ultra-light scalar saving the 3 + 1 neutrino scheme from the cosmological bounds*, *Phys. Lett.* **B797** (2019) 134911, [1907.04271].

[84] **CHARM-II Collaboration**, D. Geiregat *et al.*, *A New Determination of the Electroweak Mixing Angle From ν_μ Electron Scattering*, *Phys. Lett. B* **232** (1989) 539.

[85] **MiniBooNE Collaboration**, A. Aguilar-Arevalo *et al.*, *A Search for Electron Neutrino Appearance at the $\Delta m^2 \sim 1eV^2$ Scale*, *Phys. Rev. Lett.* **98** (2007) 231801, [0704.1500].

[86] **NOMAD Collaboration**, J. Altegoer *et al.*, *The NOMAD experiment at the CERN SPS*, *Nucl. Instrum. Meth. A* **404** (1998) 96–128.

[87] P. Minkowski, *$\mu \to e\gamma$ at a Rate of One Out of 10^9 Muon Decays?*, *Phys. Lett.* **67B** (1977) 421–428.

[88] R. N. Mohapatra and G. Senjanovic, *Neutrino Mass and Spontaneous Parity Violation*, *Phys. Rev. Lett.* **44** (1980) 912.

[89] T. Yanagida, *HORIZONTAL SYMMETRY AND MASSES OF NEUTRINOS*, *Conf. Proc.* **C7902131** (1979) 95–99.

[90] M. Gell-Mann, P. Ramond, and R. Slansky, *Complex Spinors and Unified Theories*, *Conf. Proc.* **C790927** (1979) 315–321, [1306.4669].

[91] R. N. Mohapatra, *Mechanism for Understanding Small Neutrino Mass in Superstring Theories*, *Phys. Rev. Lett.* **56** (1986) 561–563.

[92] R. N. Mohapatra and J. W. F. Valle, *Neutrino Mass and Baryon Number Nonconservation in Superstring Models*, *Phys. Rev.* **D34** (1986) 1642.

[93] M. C. Gonzalez-Garcia and J. W. F. Valle, *Fast Decaying Neutrinos and Observable Flavor Violation in a New Class of Majoron Models*, *Phys. Lett.* **B216** (1989) 360–366.

[94] P. D. Bolton, F. F. Deppisch, and P. Bhupal Dev, *Neutrinoless double beta decay versus other probes of heavy sterile neutrinos*, *JHEP* **03** (2020) 170, [1912.03058].

[95] D. Bryman and R. Shrock, *Constraints on Sterile Neutrinos in the MeV to GeV Mass Range*, *Phys. Rev. D* **100** (2019) 073011, [1909.11198].

[96] A. de Gouvêa and A. Kobach, *Global Constraints on a Heavy Neutrino*, *Phys. Rev. D* **93** (2016), no. 3 033005, [1511.00683].

[97] A. Kobach and S. Dobbs, *Heavy Neutrinos and the Kinematics of Tau Decays*, *Phys. Rev. D* **91** (2015), no. 5 053006, [1412.4785].

[98] A. Abada, A. Teixeira, A. Vicente, and C. Weiland, *Sterile neutrinos in leptonic and semileptonic decays*, *JHEP* **02** (2014) 091, [1311.2830].

[99] **BaBar Collaboration**, J. P. Lees *et al.*, *Measurement of an Excess of $\bar{B} \to D^{(*)}\tau^-\bar{\nu}_\tau$ Decays and Implications for Charged Higgs Bosons, Phys. Rev.* **D88** (2013), no. 7 072012, [1303.0571].

[100] **Belle Collaboration**, S. Hirose *et al.*, *Measurement of the τ lepton polarization and $R(D^*)$ in the decay $\bar{B} \to D^*\tau^-\bar{\nu}_\tau$, Phys. Rev. Lett.* **118** (2017), no. 21 211801, [1612.00529].

[101] **LHCb Collaboration**, R. Aaij *et al.*, *Measurement of the ratio of branching fractions $\mathcal{B}(\bar{B}^0 \to D^{*+}\tau^-\bar{\nu}_\tau)/\mathcal{B}(\bar{B}^0 \to D^{*+}\mu^-\bar{\nu}_\mu)$, Phys. Rev. Lett.* **115** (2015), no. 11 111803, [1506.08614]. [Erratum: Phys. Rev. Lett.115,no.15,159901(2015)].

[102] **LHCb Collaboration**, R. Aaij *et al.*, *Test of lepton universality using $B^+ \to K^+\ell^+\ell^-$ decays, Phys. Rev. Lett.* **113** (2014) 151601, [1406.6482].

[103] **LHCb Collaboration**, R. Aaij *et al.*, *Test of lepton universality with $B^0 \to K^{*0}\ell^+\ell^-$ decays, JHEP* **08** (2017) 055, [1705.05802].

[104] **LHCb Collaboration**, R. Aaij *et al.*, *Measurement of Form-Factor-Independent Observables in the Decay $B^0 \to K^{*0}\mu^+\mu^-$, Phys. Rev. Lett.* **111** (2013) 191801, [1308.1707].

[105] **LHCb Collaboration**, R. Aaij *et al.*, *Angular analysis of the $B^0 \to K^{*0}\mu^+\mu^-$ decay using 3 fb^{-1} of integrated luminosity, JHEP* **02** (2016) 104, [1512.04442].

[106] **LHCb Collaboration**, R. Aaij *et al.*, *Search for lepton-universality violation in $B^+ \to K^+\ell^+\ell^-$ decays, Phys. Rev. Lett.* **122** (2019), no. 19 191801, [1903.09252].

[107] D. Buttazzo, A. Greljo, G. Isidori, and D. Marzocca, *B-physics anomalies: a guide to combined explanations, JHEP* **11** (2017) 044, [1706.07808].

[108] M. Bauer and M. Neubert, *Minimal Leptoquark Explanation for the $R_{D^{(*)}}$, R_K, and $(g-2)_g$ Anomalies, Phys. Rev. Lett.* **116** (2016), no. 14 141802, [1511.01900].

[109] I. Doršner, S. Fajfer, A. Greljo, J. F. Kamenik, and N. Košnik, *Physics of leptoquarks in precision experiments and at particle colliders, Phys. Rept.* **641** (2016) 1–68, [1603.04993].

[110] **Muon g-2 Collaboration**, G. Bennett *et al.*, *Final Report of the Muon E821 Anomalous Magnetic Moment Measurement at BNL, Phys. Rev. D* **73** (2006) 072003, [hep-ex/0602035].

[111] I. Dorsner, S. Fajfer, and O. Sumensari, *Muon $g-2$ and scalar leptoquark mixing, JHEP* **06** (2020) 089, [1910.03877].

[112] E. Coluccio Leskow, G. D'Ambrosio, A. Crivellin, and D. Müller, *$(g-2)\mu$, lepton flavor violation, and Z decays with leptoquarks: Correlations and future prospects, Phys. Rev. D* **95** (2017), no. 5 055018, [1612.06858].

[113] V. Gherardi, D. Marzocca, and E. Venturini, *Low-energy phenomenology of scalar leptoquarks at one-loop accuracy, 2008.09548.*

[114] M. B. Voloshin, *On Compatibility of Small Mass with Large Magnetic Moment of Neutrino, Sov. J. Nucl.*

[115] Y. Cai, J. Gargalionis, M. A. Schmidt, and R. R. Volkas, *Reconsidering the One Leptoquark solution: flavor anomalies and neutrino mass, JHEP* **10** (2017) 047, [1704.05849].

[116] D. J. Robinson, B. Shakya, and J. Zupan, *Right-handed neutrinos and R(D(*)), JHEP* **02** (2019) 119, [1807.04753].

[117] A. Azatov, D. Barducci, D. Ghosh, D. Marzocca, and L. Ubaldi, *Combined explanations of B-physics anomalies: the sterile neutrino solution, JHEP* **10** (2018) 092, [1807.10745].

[118] D. Bečirević, N. Košnik, O. Sumensari, and R. Zukanovich Funchal, *Palatable Leptoquark Scenarios for Lepton Flavor Violation in Exclusive $b \to s\ell_1\ell_2$ modes, JHEP* **11** (2016) 035, [1608.07583].

[119] A. Angelescu, D. Bečirević, D. Faroughy, and O. Sumensari, *Closing the window on single leptoquark solutions to the B-physics anomalies, JHEP* **10** (2018) 183, [1808.08179].

[120] D. Bečirević, S. Fajfer, and N. Košnik, *Lepton flavor non universality in $b \to s\ell^+\ell^-$ processes, Phys. Rev.* **D92** (2015), no. 1 014016, [1503.09024].

[121] N. F. Bell, V. Cirigliano, M. J. Ramsey-Musolf, P. Vogel, and M. B. Wise, *How magnetic is the Dirac neutrino?, Phys. Rev. Lett.* **95** (2005) 151802, [hep-ph/0504134].

[122] M. Chala and A. Titov, *One-loop running of dimension-six Higgs-neutrino operators and implications of a large neutrino dipole moment, 2006.14596.*

[123] S. Davidson, M. Gorbahn, and A. Santamaria, *From transition magnetic moments to majorana neutrino masses, Phys. Lett.* **B626** (2005) 151–160, [hep-ph/0506085].

[124] N. F. Bell, M. Gorchtein, M. J. Ramsey-Musolf, P. Vogel, and P. Wang, *Model independent bounds on magnetic moments of Majorana neutrinos, Phys. Lett.* **B642** (2006) 377–383, [hep-ph/0606248].

[125] R. Barbieri, M. M. Guzzo, A. Masiero, and D. Tommasini, *Supersymmetry, R-parity breaking and the neutrino magnetic moment, Phys. Lett.* **B252** (1990) 251–255.

[126] K. Babu and R. N. Mohapatra, *Large transition magnetic moment of the neutrino from horizontal symmetry, Phys. Rev. D* **42** (1990) 3778–3793.

[127] J. Helo, M. Hirsch, T. Ota, and F. A. Pereira dos Santos, *Double beta decay and neutrino mass models, JHEP* **05** (2015) 092, [1502.05188].

[128] H. Päs and E. Schumacher, *Common origin of R_K and neutrino masses, Phys. Rev. D* **92** (2015), no. 11 114025, [1510.08757].

[129] C. Hagedorn, T. Ohlsson, S. Riad, and M. A. Schmidt, *Unification of Gauge Couplings in Radiative Neutrino Mass Models, JHEP* **09** (2016) 111, [1605.03986].

[130] I. Doršner, S. Fajfer, and N. Košnik, *Leptoquark mechanism of neutrino masses within the grand unification framework, Eur. Phys. J. C* **77** (2017), no. 6 417, [1701.08322].